Rock Mechanics and Rock Engineering
https://doi.org/10.1007/s00603-026-06026-5

ORIGINAL PAPER

Triaxial Testing to Determine the Shear Strength and the Shear and Normal Stiffness of Rock Joints

Charlie Chunlin Li[1] · **Ping Zhang**[2] · **Are Håvard Høien**[3]

Received: 26 May 2026 / Accepted: 21 September 2026
© The Author(s) 2026

Abstract

The mechanical properties of rock joints, including shear strength, shear stiffness, and normal stiffness, are usually determined through direct shear tests. Essentially, these properties can also be evaluated using triaxial tests performed on core specimens. One advantage of triaxial testing is that specimen deformations can be measured more readily and accurately, thereby simplifying the data acquisition process. In this study, a series of triaxial tests were performed on core rock specimens containing natural joints to evaluate the potential of triaxial testing as an alternative method for determining rock joint mechanical properties. The work included theoretical development for measuring normal and shear displacements, execution of triaxial tests, calculation of normal and shear stiffness, and analysis of the resulting data. Normal stiffness was obtained from hydrostatic triaxial tests, while the feasibility of estimating it from differential triaxial tests was also investigated. Shear stiffness and shear strength were determined from differential triaxial tests conducted under multiple confining stress levels. The results show that both normal and shear stiffness can be measured reliably using triaxial testing. The measured shear strengths align closely with Patton's bilinear failure envelope. Furthermore, the rock joint friction criterion and Patton's envelope were examined in light of the test results. These two criteria were united by deriving a relationship between the roughness angle in the friction criterion and the cohesion and residual friction angle in Patton's bilinear failure envelope.

Highlights

- Development of a triaxial testing method to determine the shear strength, as well as the shear and normal stiffness, of rock joints
- Both the theory and the testing procedure of the method, using core specimens, are proposed.
- The shear strength and shear stiffness of rock joints are determined by differential triaxial testing.
- The normal stiffness of rock joints is determined by hydrostatic triaxial testing.
- The triaxial test results of 13 rock core specimens containing natural joints are presented.

Keywords Rock joint · Shear strength · Shear stiffness · Normal stiffness · Triaxial test · Core specimen

1 Introduction

The mechanical properties of rock joints, namely shear strength, shear stiffness, and normal stiffness, are essential for stability and deformation analyses of rock joints. These properties are usually measured on direct shear testing machines (e.g., Cano et al. 2024; Wang et al. 2023; Rios-Bayona et al. 2021; Larsson 2021; Larsson and Flansbjer 2020; Sun et al. 1985; Leichnitz 1985; Barton

✉ Charlie Chunlin Li
Charlie.c.li@ntnu.no

[1] Department of Geosciences, Norwegian University of Science and Technology, Trondheim, Norway

[2] Luleå University of Technology, Luleå, Sweden

[3] Norwegian Public Roads Administration (NPRA), Bergen, Norway

Published online: 13 October 2026

and Choubey 1977; Bjurstrom 1974; Goodman and Ohnishi 1973). The procedure for direct joint shear testing is described in an ISRM Suggested Method (Muralha et al. 2014). In direct shear tests, rock joint specimens are first cast in two boxes using either cement or epoxy. After the casting material hardens, normal stress is applied to the shear boxes perpendicular to the joint surface, followed by the application of shear stress parallel to the joint surface. Shear stress is increased until slip occurs along the joint plane. The shear stress at the onset of slip is defined as the shear strength of the joint. Multiple normal stresses can be applied to a single specimen to determine the envelope of residual shear strength versus normal stress.

Triaxial testing is another alternative method for rock joint testing. Unlike conventional direct shear tests, triaxial testing of rock joints does not require casting the specimen in boxes, and the testing procedure is simpler to operate compared to direct testing. Triaxial testing of rock joints was conducted as early as in the 1960s, such as by Lane and Heck (1964), but the method has seen little use over the past half century. The triaxial tests in the early times aimed simply to determine the shear strength of rock joints, but not the normal and shear stiffness, possibly because of difficulties in the measurement of displacements within triaxial chambers. Wang and Zhu (2011) reported a study on determining the mechanical properties of rock joints by triaxial testing, but they did not provide details in their method on how to measure the shear and normal displacements of the rock joint during testing. Other current triaxial tests focus on either the behavior of intact rock or the behavior of jointed rock mass (Shan et al. 2025; Gonzalez-Fernandez et al. 2024; West et al. 2023; Arzúaa et al. 2014; Reik and Zacas 1978), but not on the measurement of mechanical properties of a single rock joint. It is worth exploring the potential of developing triaxial testing into a reliable method for determining the mechanical properties of rock joints.

A series of triaxial tests were conducted on core specimens containing a single natural joint in this study at the Rock Mechanics Laboratory of the Norwegian University of Science and Technology (NTNU). The tests aimed to develop an alternative method for determining the shear strength, normal stiffness, and shear stiffness of rock joints through triaxial testing. The theoretical basis of the method, the testing procedure, and the test results are presented in this article.

2 Theory

Under triaxial compression by axial stress σ_1 and lateral stresses $\sigma_2 = \sigma_3$, the normal and shear stresses, σ_n and τ, acting on the rock joint surface are governed by:

$$\sigma_n = \frac{\sigma_1 + \sigma_3}{2} + \frac{\sigma_1 - \sigma_3}{2}\cos 2\alpha, \tag{1a}$$

$$\tau = \frac{\sigma_1 - \sigma_3}{2}\sin 2\alpha, \tag{1b}$$

where α is the joint angle between the normal to the planar surface of the rock joint and the orientation of the major principal stress σ_1, or between the joint surface and the plane of the cross section of the core specimen (Fig. 1).

2.1 Normal Stiffness

The normal stiffness of the rock joint is determined on the normal stress–normal displacement curve of the rock joint obtained in a triaxial test under hydrostatic loading conditions, in which all three principal stresses are equal. Under these conditions, the normal stress σ_n acting on the joint surface is equal to the hydrostatic stress, i.e., $\sigma_n = \sigma_3$. The axial elastic deformation of the intact rock material within the measurement gauge length L, denoted as δ_{Le}, is expressed by:

$$\delta_{Le} = \frac{\sigma_n}{E}(1 - 2\nu)L, \tag{2}$$

where E is the Young's modulus of the rock and ν denotes Poisson's ratio.

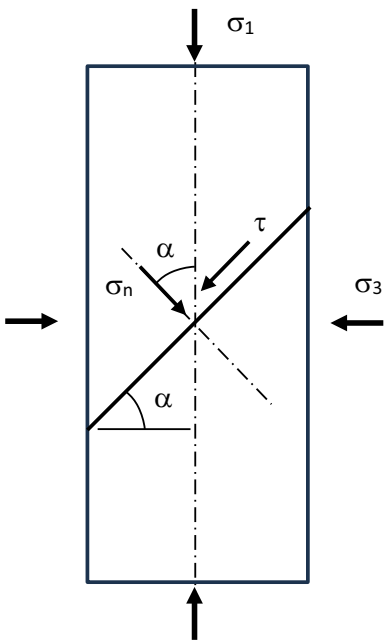

Fig. 1 A schematic illustration of the principal stresses (σ_1 and σ_3) applied to the core specimen, and the resulting normal stress (σ_n) and shear stress (τ) acting on the joint planar surface

Under hydrostatic loading conditions, shear stress on the joint surface is zero; consequently, no shear displacement develops along the joint. The total deformation of the joint is therefore in the direction of the normal to the joint, denoted as δ_{jn} in Fig. 2. This total normal joint deformation is decomposed to axial joint deformation, δ_{jna}, and lateral joint deformation, δ_{jnl}. The axial joint deformation, δ_{jna}, is expressed by:

$$\delta_{jna} = \delta_{jn} \cos \alpha. \tag{3}$$

The total axial deformation measured within the gauge length L, denoted as δ_1, is the sum of the elastic deformation of the intact rock (δ_{Le}) and the axial joint deformation (δ_{jna}). By adding Eqs. (2) and (3) and setting their sum equal to δ_1, we obtain the normal deformation of the rock joint as:

$$\delta_{jn} = \frac{1}{\cos \alpha}\left[\delta_1 - \frac{\sigma_n}{E}(1-2\nu)L\right]. \tag{4}$$

The normal stiffness of the rock joint is defined as:

$$k_{jn} = \Delta\sigma_n / \Delta\delta_{jn}. \tag{5}$$

2.2 Shear Stiffness

The shear stiffness of the rock joint is determined from the shear stress–shear displacement curve obtained in differential triaxial test, in which the axial stress σ_1 is higher than the confining stresses $\sigma_2 = \sigma_3$. Under differential loading conditions, the axial elastic deformation of the intact rock material within the gauge length L, δ_{1e}, is expressed by:

$$\delta_{1e} = \frac{L}{E}\left[\sigma_1 - 2\nu\sigma_3\right]. \tag{6}$$

The axial joint deformation, δ_{1j}, is equal to the difference between the total axial deformation within the gauge length and the elastic deformation of the rock material, that is,

$$\delta_{1j} = \delta_1 - \delta_{1e}, \tag{7a}$$

or

$$\delta_{1j} = \delta_1 - \frac{L}{E}\left[\sigma_1 - 2\nu\sigma_3\right]. \tag{7b}$$

The axial joint displacement δ_{1j} is decomposed into joint shear displacement δ_{js} and joint normal displacement δ_{jn} (Fig. 3). They are expressed as:

$$\delta_{js} = \delta_{1j} \sin \alpha = \left(\delta_1 - \delta_{1e}\right) \sin \alpha, \tag{8a}$$

and

$$\delta_{jn} = \delta_{1j} \cos \alpha = \left(\delta_1 - \delta_{1e}\right) \cos \alpha. \tag{8b}$$

The shear stiffness of the rock joint is defined as:

$$k_{js} = \Delta\tau / \Delta\delta_{js}. \tag{9}$$

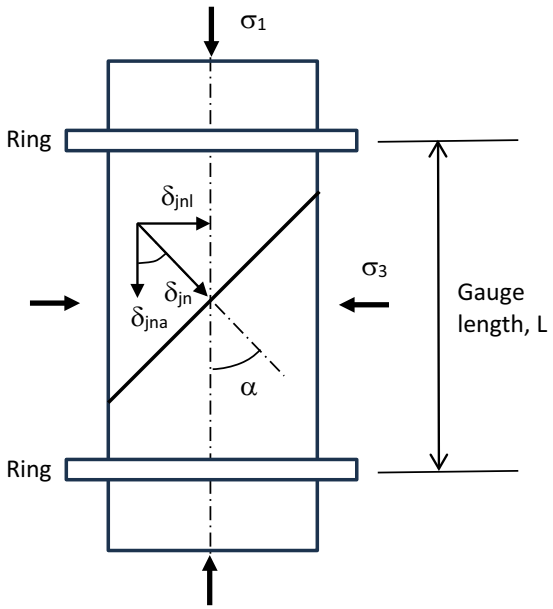

Fig. 2 A schematic illustration of the normal deformation of the joint (δ_{jn}) and its axial (δ_{jna}) and lateral (δ_{jnl}) components during hydrostatic triaxial tests. Two rings are fixed to the specimen, and the axial deformation is measured over the distance between the two rings, defined as gauge length (L)

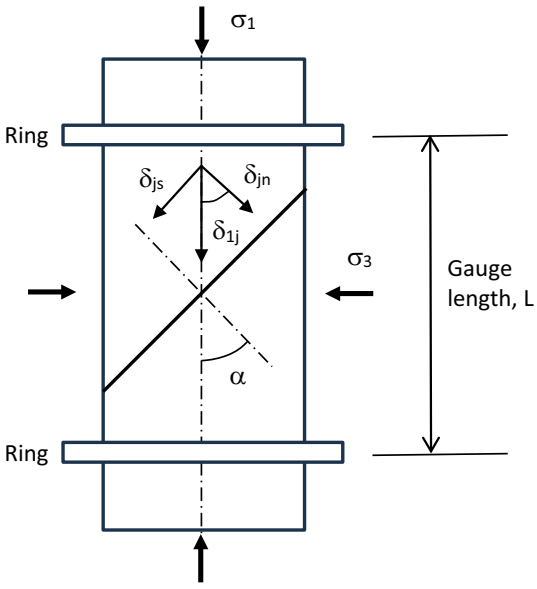

Fig. 3 A schematic illustration of the total displacement of the joint (δ_{1j}) and its normal (δ_{jn}) and shear (δ_{js}) components during differential triaxial testing

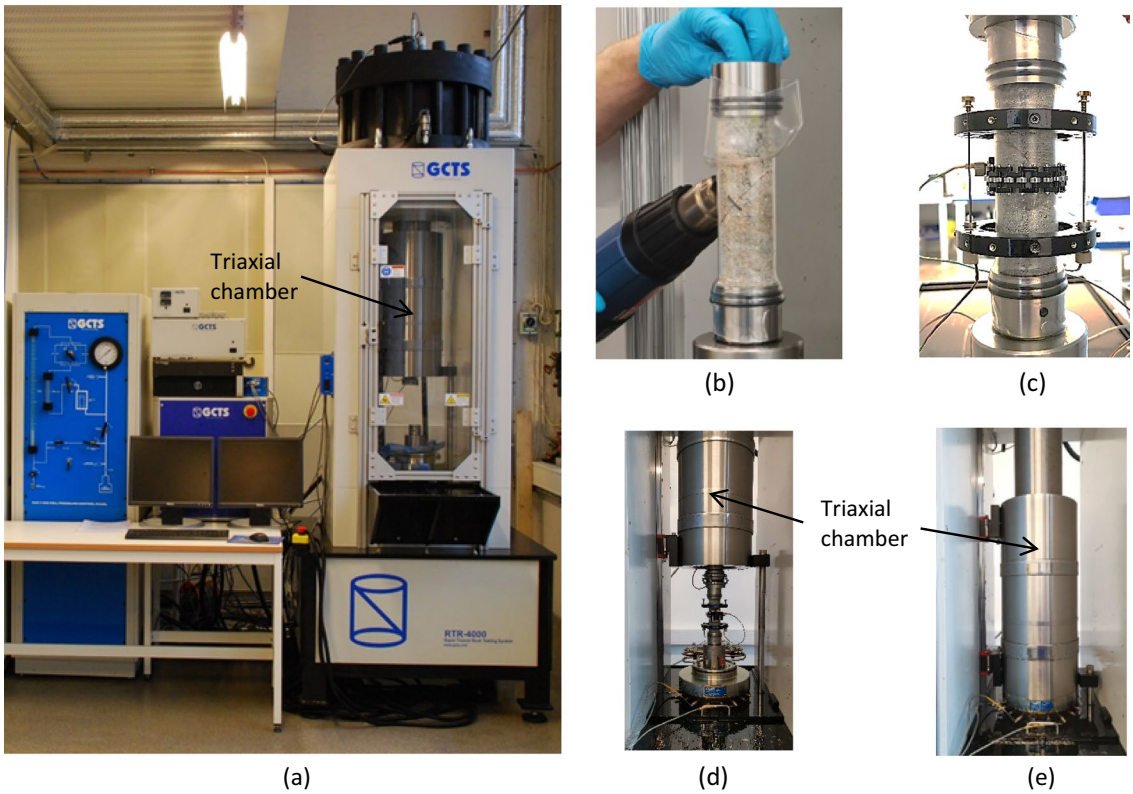

Fig. 4 The testing machine and test arrangement: **a** the GCTS RTR-4000 Rock Mechanics Testing System, **b** a core specimen under preparation, **c** a specimen equipped with LVDTs for axial and circumferential displacement measurements, **d** the opened triaxial chamber, and **e** the closed triaxial chamber ready for testing

2.3 Shear Strength

The joint slips when the shear stress τ reaches the ultimate shear resistance, that is, the shear strength s, of the joint surface in triaxial tests under differential loading conditions. The shear strength of the rock joint is expressed by (e.g., Patton 1966; Goodman 1980; Bandis et al. 1981; Barton and Bandis 1990):

$$s = \sigma_n \tan\left(\varphi_r + i\right), \tag{10}$$

where φ_r is the residual friction angle of the joint surface and i is the roughness angle. The sum of these two angles, $\varphi = \varphi_r + i$, is referred to the apparent friction angle of the joint surface.

3 Test Arrangement and Rock Specimens

3.1 Testing Machine and Test Arrangement

The triaxial tests were conducted using the GCTS RTR-4000 Rock Mechanics Testing System in the Rock Mechanics Laboratory of NTNU (Fig. 4a). The testing machine has an axial load capacity of 4000 kN, and the triaxial chamber can apply confining stresses of up to 140 MPa. The rock specimen is enclosed in a membrane (Fig. 4b). Two axial LVDTs (linear variable differential transducers) are mounted on two rings fixed to the specimen to measure the axial displacement between the rings (Fig. 4c). The distance between the rings defines the gauge length, which must fully encompass the rock joint in the middle section of the specimen. A circumferential LVDT is installed at mid-height of the specimen, and the circumferential displacement is used as feedback to control the loading process during differential triaxial testing. After the specimen is instrumented with the LVDTs, it is placed inside the triaxial chamber (Fig. 4d and e), which is then filled with oil.

In the triaxial test under hydrostatic loading conditions, the specimen is fully immersed in oil. The oil pressure is slowly increased to the predefined confining stress σ_3, while the axial displacement within the gauge length is recorded.

In the triaxial test under differential loading conditions, the oil pressure is first increased to the predefined confining stress, σ_3. The axial stress, σ_1, is then increased from the level of σ_3 until a plateau is reached, indicating that the shear strength of the rock joint has been mobilized and slip has occurred. Subsequently, the confining stress is

increased to a higher level, after which σ_1 is raised again until the next plateau is reached. This procedure is repeated until the target level of σ_3 has been attained. The purpose of this testing sequence is to determine the shear strength and shear stiffness of the rock joint under different normal stresses. In addition, some specimens are reassembled and retested following the first test run to investigate changes in the mechanical properties of the rock joint resulting from damage and unloading.

3.2 Rock Specimens

The rock core samples were collected from boreholes KBH 1 and KBH 2 that were drilled in Bratteråas, Gothenburg in Sweden. Hole KBH 1 was drilled in the azimuth of 40° in a plunge of −5° (downward). Hole KBH 2 was drilled in the azimuth of 215° in a plunge of −1° (downward). The core diameter was 45 mm. The rock type was mainly granitic diorite. Both intact rock specimens and specimens containing a single joint were prepared for testing. Based on the rock color, the specimens were divided into three groups: pink (Group A), red (Group B), and gray (Group C). The specimens in each group, together with their corresponding test type, are listed in Table 1.

The intact rock specimens were used to determine the mechanical properties of the rocks. The tests were conducted following the instructions in the suggested method by Bieniawski and Bernede (1979). The rock joint specimens were used in hydrostatic and differential triaxial tests for determining the mechanical properties of the rock joints. In both hydrostatic and differential triaxial tests, two LVDTs were used to measure the axial displacement within the gauge length between two rings fixed on the specimen (Fig. 5). The rock joint must be entirely encompassed within the gauge length. All intact and joint specimens except B2 and C3 were 135 mm long and had a gauge length of 79.3 mm. Specimens, B2 and C3, had a length of 150 mm and a gauge length of 104.9 mm to accommodate the joint lengths. The joint angles of the specimens are presented in Table 1. Figure 6 presents rock joint specimen A1 and its joint surface before and after testing. Such images of all other joint specimens are presented in Appendix A.

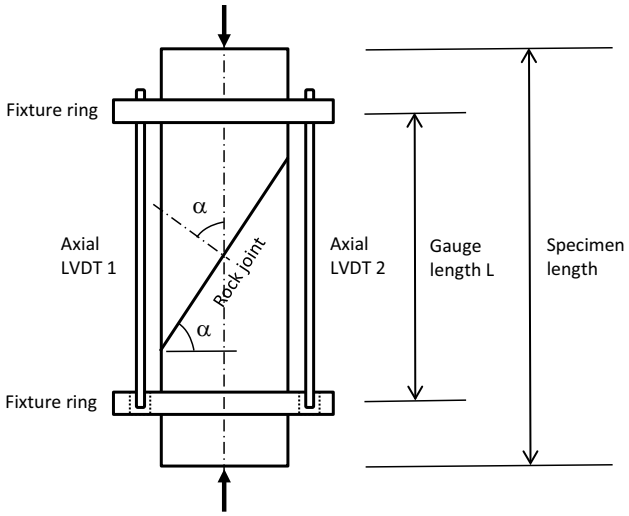

Fig. 5 A schematic illustration of the installation of axial LVDTs on a rock joint specimen, showing the gauge length and specimen length

4 Test Results

4.1 Mechanical Properties of the Intact Rock

Four intact rock specimens were tested under uniaxial compression to determine the uniaxial compressive strength

Table 1 Diorite specimens of 45 mm in diameter

Spec group	Spec. no.	Spec type	Joint angle α (°)	Hydrostatic triaxial test	Differential triaxial test	UCS test
A: Pink	A1	Rock joint	54.9	Yes	Yes	–
	A2		48.6	Yes	Yes	–
	A3		46.9	Yes	Yes	–
	A4	Intact rock	–	–	–	Yes
	A5		–	–	–	Yes
B: Red	B1	Rock joint	50.2	Yes	Yes	–
	B2		62.7	Yes	Yes	–
C: Gray	C1	Rock joint	45.0	Yes	Yes	–
	C2		20.7	Yes	Yes	–
	C3		60.9	–	Yes	–
	C4		49.7	Yes	Yes	–
	C5	Intact rock	–	–	–	Yes
	C6		–	–	–	Yes

Fig. 6 Specimen A1 (joint angle $\alpha = 54.9°$): **a** the rock joint specimen, **b** the joint surface before test, **c** the joint surface after the first test run, and **d** the joint surface after the second test run

Table 2 The measured mechanical properties of the intact rock specimens

Spec No	UCS (MPa)	E (GPa)	ν
A4	149.8	76.3	0.27
A5	169.7	77.8	0.29
C5	180.5	81.9	0.29
C6	–	80.0	0.25

(UCS), the Young's modulus (E), and Poisson's ratio (ν) of the intact rocks. Their results are presented in Table 2.

The average values of the Young's modulus and Poisson's ratio are 77 GPa and 0.28 for Group A rock and 81 GPa and 0.27 for Group C rock. Owing to the similarity between the Group A and Group B rocks, the mechanical properties determined for Group A were used in the calculations involving Group B specimens in the subsequent sections.

4.2 Normal Stiffness of the Rock Joint

In the hydrostatic triaxial tests for determining the normal stiffness of the rock joint, the specimen was placed in the triaxial chamber and the oil pressure in the chamber was increased to 10 MPa at a constant rate of 0.8 MPa/min. Because the specimen was entirely immersed in oil in this test, the stresses exerted to the specimen are equal to oil pressure in all orientations. During loading, the axial displacement of the specimen within the gauge length, δ_1, was measured. The normal displacement of the rock joint was

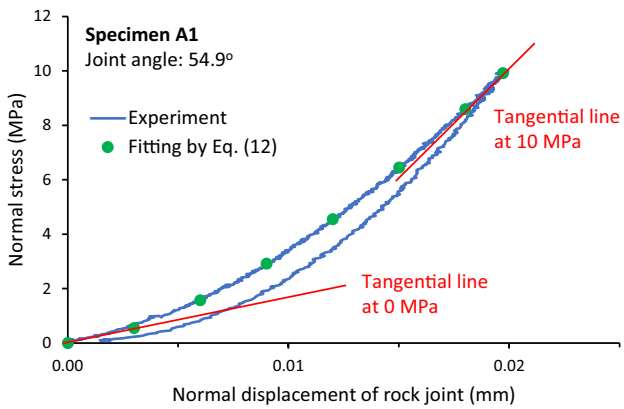

Fig. 7 Specimen A1: normal stress versus normal displacement and tangential lines at 0 and 10 MPa

calculated from δ_1 according to Eq. (4). Figure 7 shows the curve of normal stress versus normal displacement of specimen A1 during a loading and unloading cycle. The curves of the other specimens are presented in Appendix B. The slope of the tangential line on the curve represents the normal stiffness of the rock joint. The normal stiffness at a given normal stress is calculated using the increments in normal stress and normal displacement according to Eq. (5). The slopes of the two red lines in Fig. 7 represent the normal stiffness of the rock joint in A1 at normal stresses 0 and 10 MPa. The normal stiffness of the rock joint at these two stress levels is calculated for all tested specimens and their values are presented in Table 3. The green dots on the loading portion of the curve in Fig. 7 represent the regression

Table 3 The values of the normal stiffness of the rock joints in the tested specimens

Rock type	Spec	Normal stiffness (GPa/m)	
		$\sigma_n = 0$ MPa	$\sigma_n = 10$ MPa
Group A	A1	170	800
	A2	33	150
	A3	127	440
Group B	B1	140	435
	B2	215	1060
Group C	C1	50	250
	C2	145	381
	C4	70	149

trajectory of the experiment data, which will be discussed in detail in Sect. 5.1.

4.3 Shear Stiffness of the Rock Joint

In the tests for determining the shear stiffness of the rock joint, the confining stress σ_3 of a predefined level was applied to the specimen by increasing the oil pressure in the triaxial chamber. After that, the axial stress was increased by moving downward the piston of the actuator under radial strain control by applying a radial strain rate of approximately 10 micro strains ($\mu\varepsilon$) per second. The axial displacement within the gauge length was measured during loading. The axial stress continued to increase until the rock joint started to slip, which was marked by an approximately constant axial stress with increasing axial displacement. The confining stress was then lifted to a higher level, and the axial stress was raised again until the next constant axial stress level was reached. The test was terminated after three to five confining stress levels had been applied to the specimen. Some of the specimens were tested in more than one run. The shear stress on the joint was calculated from the axial stress and confining stress using Eq. (1b), and the shear displacement was calculated using Eq. (8a). Figure 8 shows the shear stress–shear displacement curves of specimen A1 that was tested in two runs under various confining stresses. In the first run, the constant shear stress, representing the shear strength of the rock joint, was not reached. In the second run, the shear stress reached the level of shear strength under all applied confining stress levels. The red lines in the diagrams are the tangential lines to the linear rising portion of the curve for each confining stress. The shear stiffness of the joint is calculated from the red line at each confining stress level according to Eq. (9). The shear stress–shear displacement curves of the other specimens are presented in Appendix C. The values of the shear stiffness calculated for all specimens are presented in Table 4. The curve portion where the shear stiffness is determined corresponds to

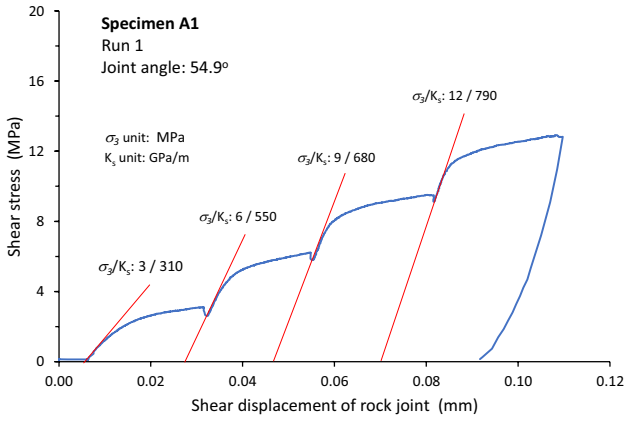

(a)

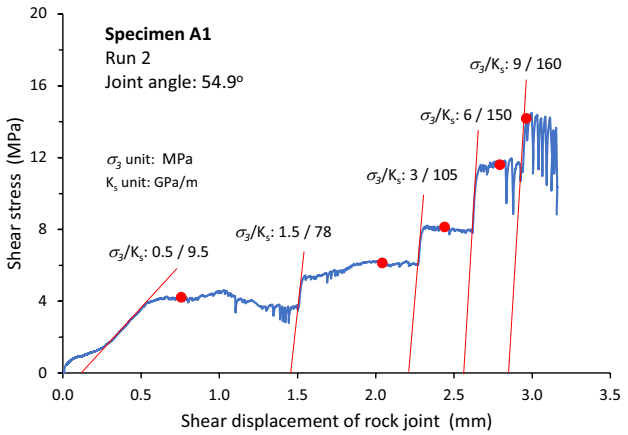

(b)

Fig. 8 Shear stress–displacement curves of specimen A1 under various confining stresses from two test runs: **a** the first run and **b** the second run. The red lines in the diagrams are used to calculate the shear stiffness of the joint at each confining stress level

a range of normal stresses on the joint plane. The normal stress range is also presented in Table 4. The joint angle of specimen C2 is 20.7°, which is less than the friction angle of the joint surface (greater than 30° as presented later). The joint did not slip, so this specimen was excluded from the table.

4.4 Shear Strength of the Rock Joint

The rising shear stress of most of the specimens gradually reached a plateau level with increasing shear displacement, as shown in Fig. 8b. However, for specimens B2 and C3 which had relatively rough joint surfaces, the shear stress reached a peak value first and then dropped to a lower plateau level under the first applied confining stress, as shown in Fig. 36 and Fig. 39a. Under the subsequent higher confining stress levels, the shear stress gradually increased

Table 4 The values of the shear stiffness of the rock joints obtained in the tests (units: k_s in GPa/m and σ_n in MPa)

Spec. No	Test run	σ_3 = 0.5 MPa		σ_3 = 1.5 MPa		σ_3 = 3 MPa		σ_3 = 6 MPa		σ_3 = 9 MPa		σ_3 = 12 MPa	
		σ_n	k_s	σ_n	k_s	σ_n	k_s	σ_n	k_s	σ_n	k_s	σ_n	k_s
A1	1					0.2–3.9	310*	7.9–9	550*	13.2–14.3	680*	15.5–19.5	790*
	2	1.5–3	9.5	2.9–5.1	78	6–8.5	105	11–13.5	150	14–18	160		
A2								6–8	120*				
A3	1					3–6.3	430*	16.5–18	790*	23.5–24.5	780*	30–31	790*
	2	0.6–3	33	10–12	90	13.5–16	220						
	3					3.1–5.3	85	18.5–24	350	27–32.5	350	38–41	350
B1	1							6.5–22	305 335 300				
B2	1					3.5–7	300*	8–11.5	165	13.5–16	165	17–21	165
C1	1	0.7–4.5	45	7–9	170	9–13	170	14–18	170	20–25	170		
C3	1	0.7–4	2800*	3–4	240	4.5–7	240	7.5–12	240	12–16	240		
	2					3.2–4.5	125	8–11.5	190	12–15.5	190	17–21	190
C4	1					3.2–4.5	130*	8.5–9	100	14.5–15	120	20.5–21	125
	2			3.5—4.5	50	5.5–7.5	55	6.5–8.5	95, 90	17–20	130	12.5–16	170

*Slip did not occur along the joint surface

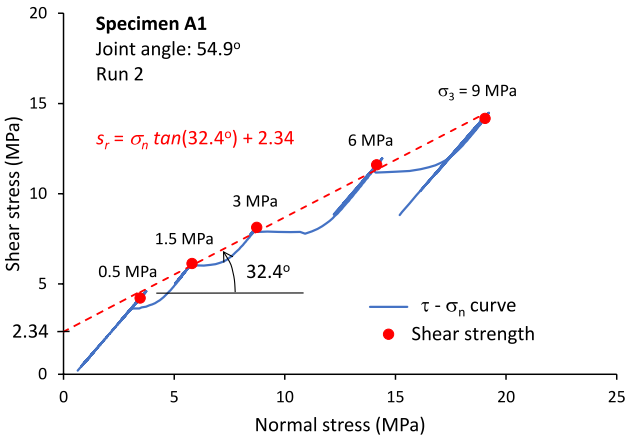

Fig. 9 Shear stress versus normal stress on the joint plane of specimen A1 during the second test run

Table 5 Friction angle and cohesion of the rock joint back-calculated from test results

Spec No	Res. friction angle φ_r (°)	Cohesion (MPa)
A1	32.4	2.34
A3 (run 2)	36.9	2.53
A3 (run 3)	35.0	3.52
B2	36.7	2.71
C1	30.3	2.23
C3 (run 1)	37.7	1.82
C3 (run 2)	34.0	2.84
C4	32.8	1.14

and eventually reached a plateau without exhibiting a peak. It is believed, therefore, that the plateau stress level represents the residual shear strength of the rock joint. Shear strength is identical to residual shear strength in this article. The shear stress did not reach the plateau level in the first test run of specimens A1, A3, and C4 (see Fig. 8a, Fig. 34a and Fig. 40a). Those runs were discarded in the determination of the shear strength. The shear and normal stresses during loading were calculated from the prevailing axial stress σ_1 and the confining stress σ_3 using Eq. (1). Figure 9 shows the curve of shear stress versus normal stress on the joint surface of specimen A1 during the second test run as well as the shear strengths corresponding to the individual confining stresses, which are marked by red points in the diagram. The relationship between the shear strength of rock joint and the normal stresses can be well described by the following linear regression expression:

$$s = \sigma_n \tan \varphi_r + c, \tag{11}$$

where s is the shear strength of the rock joint, σ_n the normal stress on the joint surface when slip occurs, φ_r the slope angle of the regression trendline for the shear strength, and c the cohesion of the rock joint. For the second test run of specimen A1, the residual friction angle obtained from the regression of the experimental data is $\varphi_r = 32.4°$, and the cohesion $c = 2.34$ MPa, as marked in Fig. 9. The curves of shear stress versus normal stress for the other specimens are presented in Appendix D. The residual friction angle and the

cohesion for those specimens were obtained with the same method as described above. Their values are summarized in Table 5. It can be seen in Table 5 that the residual friction angles of specimens A3 and C3, both of which were subjected to multiple test runs, decreased in the second test run. The residual friction angle is generally considered to consist of the basic friction angle and a residual roughness angle, the latter being dependent on the degree of asperity damage. During the first test run, the joint surfaces experienced asperity degradation, which reduced the residual roughness angle. Consequently, the residual friction angle decreased in the second test run.

5 Analysis and Discussion

5.1 On Normal Stiffness

Goodman (1976) proposed a hyperbolic expression to describe the relationship between normal stress and normal joint displacement as follows:

$$\frac{\sigma_n - \xi}{\xi} = A\left(\frac{V}{V_{\max} - V}\right)^t,$$

where ξ is the initial normal stress at which the measured normal displacement is $V = 0$, and $V_{\max}$ is the maximum closure displacement of the rock joint. The above equation is not valid for the case of zero initial normal stress. Instead, the relationship should be expressed in the following form:

$$\sigma_n = R\left(\frac{V}{V_{\max} - V}\right)^t. \tag{12}$$

The normal stress–normal displacement curves of the rock joint specimens were fitted using Eq. (12) by adjusting the three constants, R, $V_{\max}$, and t. The best fitting results are shown by the green dots in Fig. 7 and the figures in Appendix B. The values of the three constants for the individual specimens are presented in Table 6.

Equation (12) describes the normal stress–normal displacement behavior of rock joint satisfactorily. The constants in the equation are empirical regression parameters and do not have clearly defined physical or mechanical interpretations. However, based on their influence on the shape of the fitted curve, R appears to be related to the actual contact area, $V_{\max}$ to the initial opening of the joint and t to the elasticity of the joint surface. The values of t for all specimens except A3 and C4 are 1.5, indicating that the elasticity of the joint surface is similar in those specimens.

The normal stiffness k_n of the rock joint can be obtained by differentiating the normal stress σ_n with respect to the normal joint displacement V in Eq. (12), that is,

Table 6 The values of the constants in Eq. (12) for all rock joint specimens

Rock type	Spec No.	Constants in Eq. (12)			k_n (GPa/m) at $\sigma_n = 10$ MPa by Eq. (13)
		R (GPa/m)	V_{max} (mm)	t	
Group A	A1	680	0.35	1.5	802
	A2	320	1.5	1.5	122
	A3	110	0.3	1.2	380
Group B	B1	190	0.3	1.5	463
	B2	45	0.06	1.5	1273
Group C	C1	38	0.3	1.5	242
	C2	2800	1.7	1.5	395
	C4	31	0.35	1.1	162

$$k_n = \frac{d\sigma_n}{dV} = RtV_{\max}\frac{(V)^{t-1}}{\left(V_{\max} - V\right)^{t+1}}. \tag{13}$$

The normal stiffness calculated for the specimens using Eq. (13) is presented in the last column in Table 6. They match well with the manually calculated normal stiffness values presented in Table 3.

For the specimens with $t = 1.5$, the normal stress and normal stiffness of the rock joint can be expressed as:

$$\sigma_n = R\sqrt{\left(\frac{V}{V_{\max} - V}\right)^3},$$

$$k_n = \frac{2RV_{\max}}{3\left(V_{\max} - V\right)^2}\sqrt{\frac{V}{V_{\max} - V}}.$$

In principle, the variation in the normal stiffness of a rock joint during differential loading can also be determined from the normal stress acting on the joint surface and the corresponding normal joint displacement. During differential triaxial testing, the normal stress on the joint is calculated from the axial stress and confining stress using Eq. (1a). The normal joint displacement, $\rightharpoonup_{jn}$, is calculated according to Eq. (8b).

Taking specimen A1 as an example, Fig. 10 presents the normal stress–normal displacement relationship obtained during the second run of the differential triaxial testing. The steep portions of the curve, marked by the red lines, represent the elastic normal deformation of the rock joint under the corresponding confining stresses prior to shear slip along the joint surface. In contrast, the plateau portions correspond to relative rigid-body movement of the upper and lower pieces of the specimen during shear slip along the joint. The normal stiffness of the rock joint can be determined only from the steep portions of the curve before shear slip occurs. Based on Eq. (5), the calculated

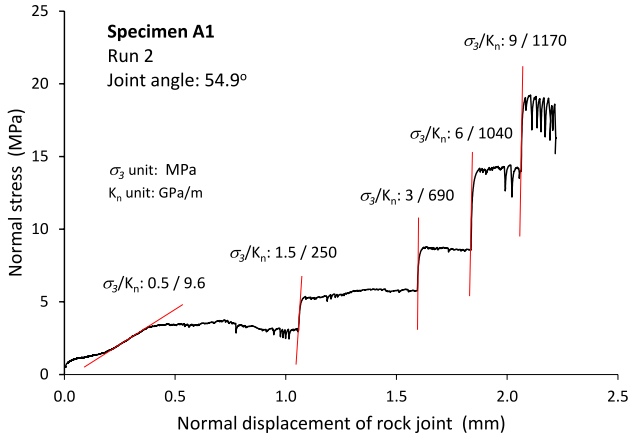

Fig. 10 Normal stress–normal displacement curve of specimen A1 under various confining stresses from the second test runs. The red lines in the diagrams are used to calculate the normal stiffness of the joint at each confining stress level

normal stiffness values are 9.6 GPa/m at $\sigma_3 = 0.5$ MPa, 250 GPa/m at $\sigma_3 = 1.5$ MPa, 690 GPa/m at $\sigma_3 = 3$ MPa, 1040 GPa/m at $\sigma_3 = 6.$ MPa, and 1170 GPa/m at $\sigma_3 = 9$ MPa. The joint normal stiffness is lowest at the initial confining stress of 0.5 MPa, possibly due to an imperfect match between the opposing joint surfaces at the beginning of the second test run. Following the test under the confining stress of 0.5 MPa, the joint surfaces came into closer contact, resulting in a substantial increase in normal stiffness.

Overall, the results indicate that joint normal stiffness generally increases with increasing normal stress acting on the joint surface. The normal stiffness values obtained from the differential triaxial tests, with the exception of the value measured at the initial confining stress of 0.5 MPa, are higher than those derived from the hydrostatic triaxial testing. For example, the joint normal stiffness of specimen A1 was only 800 GPa/m at a normal stress of $\sigma_n = 10$ MPa in the hydrostatic triaxial test (Table 3), whereas a value of approximately 1040 GPa/m was obtained at the same normal stress level in the triaxial test (Fig. 10). One possible explanation for this discrepancy is that the joint surface experienced damage and progressive asperity degradation during the differential triaxial testing. As a result, the opposing joint surfaces became smoother and achieved a better mechanical fit, leading to a stiffer normal response and, consequently, higher apparent normal stiffness values. In contrast, the joint normal stiffness of specimen A1 was 170 GPa/m at $\sigma_n = 0$ MPa in the hydrostatic test (Table 3), which is substantially higher than the value of 9.6 GPa/m measured at $\sigma_n = 0.5$ MPa during the second triaxial test run (Fig. 10). This discrepancy may be attributed to differences in surface roughness and the degree of matching between the opposing joint surfaces. The joint roughness had already been partially degraded during the first triaxial test run, and the opposing surfaces may have exhibited a poorer fit in the subsequent triaxial test than in the hydrostatic test. Consequently, the normal stiffness measured at the first confining stress of 0.5 MPa in the triaxial test was lower.

Similar analyses were performed for the other specimens; however, the results were not as consistent as those obtained for specimen A1. A major limitation of the method is that the steep portions of the normal stress–normal displacement curves are often very short, making it difficult to derive reliable estimates of normal stiffness. Consequently, caution must be required when applying this approach to determine the normal stiffness of rock joints in differential triaxial tests.

In contrast, hydrostatic triaxial testing provides a more reliable means of determining the normal stiffness of rock joints, as it enables the normal stress–normal displacement response to be measured directly under controlled loading conditions. Therefore, hydrostatic triaxial testing is generally recommended when accurate characterization of joint normal stiffness is required.

5.2 On Shear Stiffness

For most specimens, the joint shear stiffness is the lowest under the first confining stress during the first test run. This may be attributed to loose matching between the opposing surfaces of the rock joint at the beginning of the test. Under subsequent elevated confining stresses, the shear stiffness increases significantly, as demonstrated in Fig. 8 and the plots presented in Appendix C. This increase may be attributed to improved matching at the actual contact points following asperity damage. Thereafter, shear stiffness generally shows a slight increase with increasing confining stress, beginning from the second confining stress level within the same test series. Exceptions were observed for specimens B2 and C3, for which the joint shear stiffness was highest under the first confining stress during the first test run. This behavior may be explained by a better initial match and stronger interlocking between the joint surfaces prior to asperity degradation. It was also observed that the shear stiffness was lower in the subsequent test run than in the preceding test run under similar normal stress conditions, as exemplified by specimen C3 (Table 4). This reduction in shear stiffness may be attributed to differences in the degree of asperity damage developed during the two test runs. The joint surface likely underwent asperity degradation during the preceding test run, resulting in reduced surface roughness and weaker interlocking between the opposing joint surfaces. Consequently, the shear stiffness decreased in the subsequent test run.

If the specimen is reassembled and retested after the first test run, the shear stiffness generally becomes significantly lower than that observed during the initial run, as exemplified by specimens A1 and A3 in Table 4. This reduction

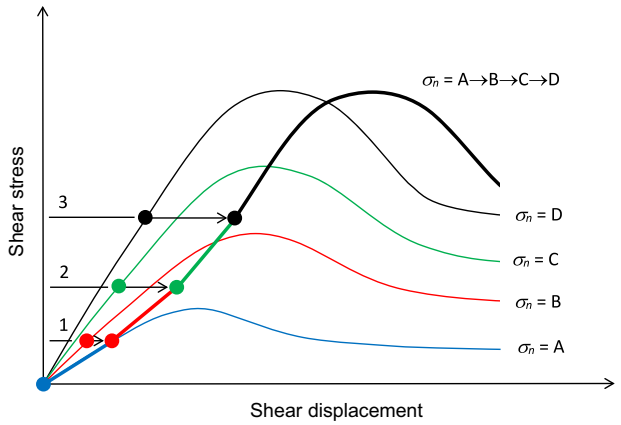

Fig. 11 A Schematic illustration of the shear stress versus shear displacement under constant and varying normal stresses

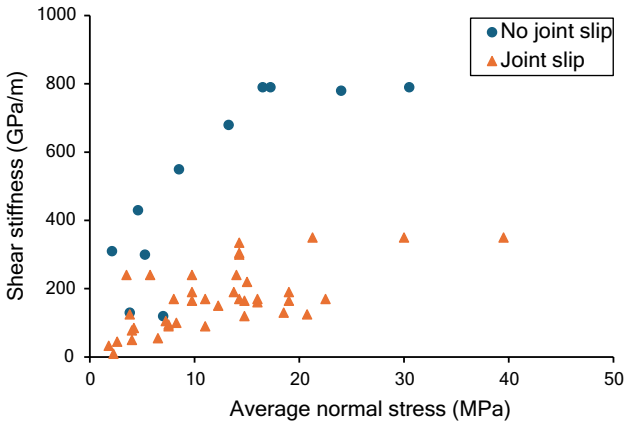

Fig. 12 Scatter plots of shear stiffness versus average normal stress on the joint surface

in stiffness may be attributed to imperfect matching of the softened surfaces created by damage during the first test run.

Previous studies have shown that shear stiffness increases with increasing normal stress on the rock joint (e.g., Goodman 1980; Bandis et al. 1983; Sun et al. 1985; Grasselli and Egger 2003; Muralha et al. 2014; Zhang et al. 2016). Assume that the thinner lines in Fig. 11 represent the shear stress–shear displacement curves, obtained in four tests under different constant normal stresses with A < B < C < D. Let us imagine conducting a test by raising the normal stress from A to B, C, and D at different shear stress levels during testing, and see how the shear stress–shear displacement curve is changed. The shear test starts with normal stress σ_n = A and the normal stress is raised to B at stress level 1, to C at level 2, and finally to D at level 3. The shear stress increases from zero following curve σ_n = A until level 1. Then, it follows curve σ_n = B until level 2, curve σ_n = C until level 3, and finally curve σ_n = D until the end of the test. The thicker line represents the complete shear stress–shear displacement path under these four varying normal stresses. The overall slope of the curve before yielding represents the average shear stiffness under the four normal stresses.

The normal stress on the rock joint in the differential triaxial tests was not constant, but it increased with the shear stress. The shear stiffness determined in the tests was for the upper linear part of the curve which corresponds to a narrow range of normal stresses as presented in Table 4. Figure 12 shows the shear stiffness of the specimens plotted against the average normal stress over the range in which the shear stiffness was determined. The blue solid circles represent tests in which the rock joints did not slip, indicating no or only very slight surface damage (i.e., the values marked with stars in Table 4), whereas the orange triangles represent tests in which the rock joints experienced slip, indicating surface damage. The data in both categories show similar trends: shear stiffness increases with increasing normal stress up to 15 MPa. Above 15 MPa, the shear stiffness remains essentially constant.

5.3 On Shear Strength

For a rock joint specimen tested under triaxial compression, Goodman (1980) introduced a Mohr circle method to graphically determine the shear strength and the normal stress on the joint plane when shear failure occurs (Fig. 13). With this method, a Mohr circle is constructed in a diameter of (σ_1–σ_3) with its center on the axis of normal stress, where σ_3 is the applied confining stress and σ_1 is the ultimate axial stress obtained in the test. A line is then drawn from the point representing σ_3 upward in the angle of the rock joint, α. The point of intersection between the drawn line and the Mohr circle represents the shear strength of the rock joint and the corresponding normal stress acting on the joint surface at the onset of shear failure. The same values of shear strength and normal stress can be obtained by substituting the values of α, σ_1, and σ_3 into Eq. (1).

As an example, Fig. 14 shows the application of the Mohr circle method to determine the residual shear strengths of specimen B2 corresponding to four confining stresses applied in the tests.

It is commonly assumed that the ultimate shear resistance of a rock joint is governed solely by friction along the joint surface, with cohesion assumed to be zero. In general, cohesion refers to the tendency of materials to stick together or remain united. In physics, cohesion is the force that holds similar molecules together. A rock joint consists of two surfaces that are often separated and only come into contact at a limited number of points. These surfaces have either no bond at all or only very weak bond in some cases. Therefore, it is reasonable to assume zero cohesion for rock joints. However, regression analysis of test results from many studies (e.g., Patton 1966; Zhao 1997), as well as from our study as shown

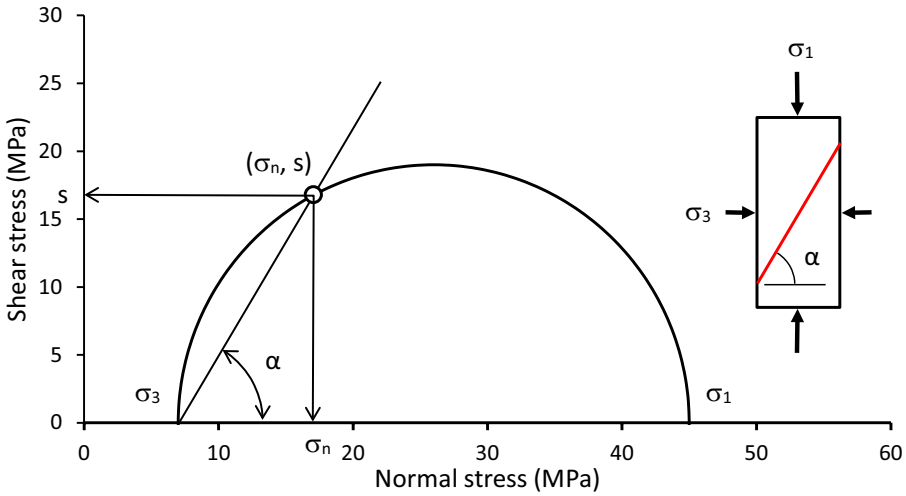

Fig. 13 Mohr circle method for determining the normal stress and shear strength based on the confining stress σ_3 and the maximum axial stress σ_1

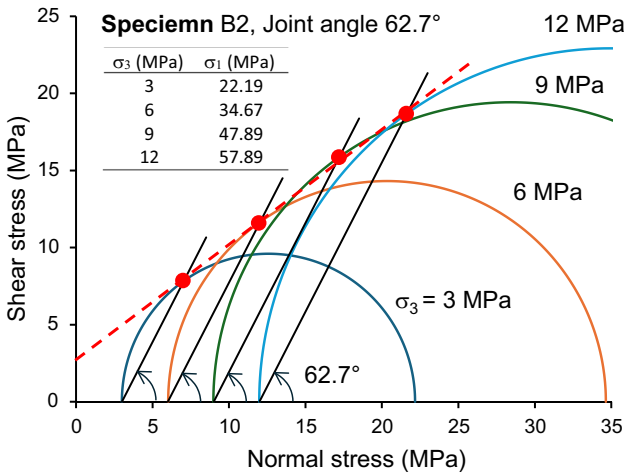

Fig. 14 The residual shear strength of specimen B2 determined by the Mohr circle method

in Fig. 9, indicates that shear strength is linearly related to normal stress, with a non-zero cohesion once normal stress exceeds a certain threshold. This apparent inconsistency between the test results and the expected zero cohesion behavior may be explained by the contact conditions of the joint surface during shearing.

The topography of a rock joint can be characterized by large-scale undulations and local asperities, as illustrated in Fig. 15a. The joint remains interlocked due to these local asperities in the beginning until the shear stress exceeds a certain limit. Beyond this point, relative displacement occurs between the opposing surfaces of the joint, and the forces are transferred through only a limited number of contact points, as observed on the joint surfaces of specimen A1 after testing, shown in Fig. 6d. The rock material at these contact points undergoes crushing and flattening under elevated contact stress (Fig. 15b). Subsequently, the residual shear strength of the joint is governed by two components: frictional resistance along the actual contact surfaces and interlocking resistance at the contact points. The frictional resistance is governed by the residual friction angle, defined as

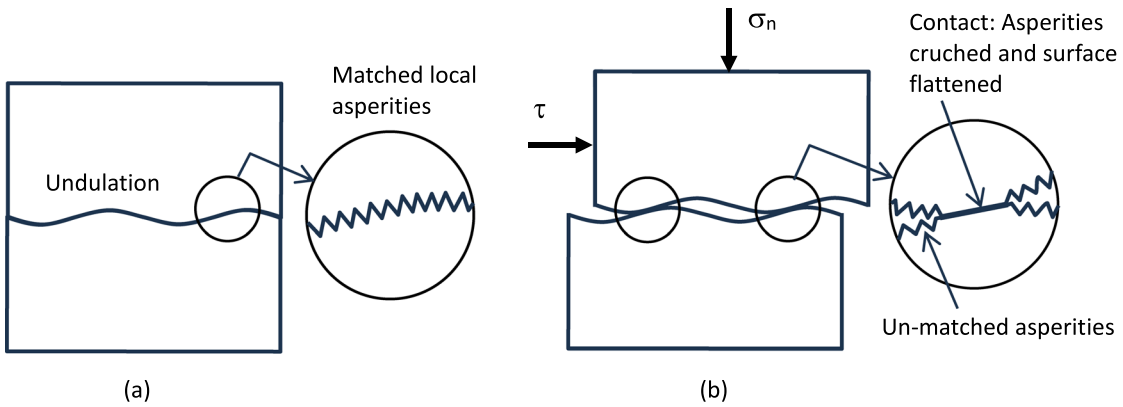

Fig. 15 Sketches illustrating **a** matched local asperities on a joint surface under unloaded condition and **b** point contacts after a certain shear movement under shear and normal loading

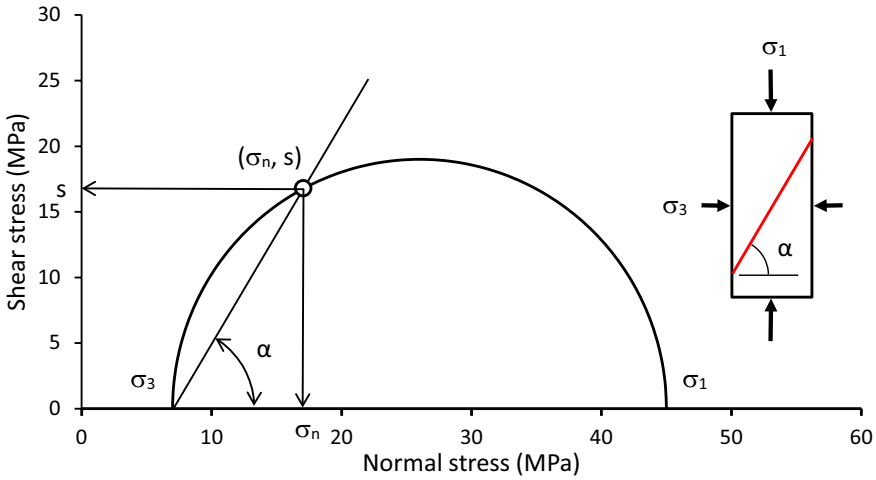

Fig. 16 Bilinear shear failure envelope for hard rock joints

the sum of the basic friction angle and the average inclination angle of the joint undulation. For a given undulation scale, the residual friction angle remains constant; however, it generally decreases as the scale increases. The interlocking resistance can be attributed not only to the large-scale undulating topography of the joint surface but also to the micro-asperities within the actual contact areas and to the initial asperities located along the boundaries of these contact areas. Therefore, the so-called cohesion, c, in Eq. (11) does not represent cohesion in the physical sense. Rather, it is a parameter that characterizes the shear interlocking effect arising from the surface geometry and asperity interactions of the rock joint.

Patton (1966) conducted a series of direct shear experiments on specimens fabricated from artificial materials. The specimens consisted of matching triangular asperities with inclination angles (i_0) of 25°, 35°, and 45°, respectively. The residual friction angle (φ_r) of the material was determined from shear tests conducted on sawn surfaces and was found to be approximately 30°. The test results obtained from specimens with matching triangular asperities demonstrated that, under low normal stresses, the joint shear strength increased along a relatively steep linear trend with a slope of $\left(\varphi_r+i_0\right)$, provided that the asperities remained intact. In contrast, under high normal stresses, the asperities were sheared off, causing the shear strength to follow a flatter linear trend characterized by a slope of φ_r. This behavior results in a bilinear shear strength envelope, as illustrated in Fig. 16, which can be expressed as:

$$s = \sigma_n \tan\left(\varphi_r + i_0\right), for \sigma_n \le \sigma_{n0}, \tag{14a}$$

$$s = \sigma_n \tan\varphi_r + c, for \sigma_n \ge \sigma_{n0}, \tag{14b}$$

where σ_{n0} represents the critical normal stress at which intact asperities begin to experience damage. The test results obtained from rock core specimens containing matching natural joints, as shown in Fig. 9 and Appendix D, are in good agreement with the linear trend expressed by Eq. (14b). The steeper linear trend, expressed by Eq. (14a), was not observed in the present tests, possibly because the applied normal stresses were too high to preserve intact asperity behavior. Nevertheless, based on the underlying shear mechanism and the findings of Patton (1966), it is reasonable to infer that a steeper trend line would also exist for matching natural rock joints under sufficiently low normal stresses. Therefore, Eq. (14) is considered applicable to hard natural rock joints, where i_0 denotes the initial roughness angle of the joint surface.

Equations (10) and (14) describe the same shear failure envelope, although they express it in different forms. The two formulas are united if the roughness angle i is expressed by the cohesion and residual friction angle as follows:

$$i = \arctan\left(\tan\varphi_r + \frac{c}{\sigma_n}\right) - \varphi_r. \tag{15}$$

Figure 17 graphically shows the variation of roughness angle versus the ratio of cohesion to normal stress over a range of the residual friction angle from 20° to 45°. Equation (15) is valid for $c/\sigma_n < c/\sigma_{n0}$. Above c/σ_{n0}, the roughness angle remains constant at i_0, and slip occurs along the surface of asperities without asperity damage. The value of c/σ_{n0} can be obtained from Eq. (15) by setting $i = i_0$. For example, by letting $\varphi_r = 35°$ and $i_0 = 20°$, Eq. (15) gives $c/\sigma_{n0} = 0.73$. The thick blue line in Fig. 17 represents the variation of i with the ratio c/σ_n for this example.

The test results of our study indicate that the residual friction angle decreases and the cohesion increases with increasing damage of the joint surface. For example, specimens A3 and C3 exhibited a decrease in friction angle and an increase in cohesion in subsequent tests compared with the preceding test run, as shown in Table 5. Those changes are logically reasonable.

The purpose of the above analysis is simply to unify the two criterion expressions, Eq. (10) and Eq. (14), by establishing a relationship between their respective parameters. It

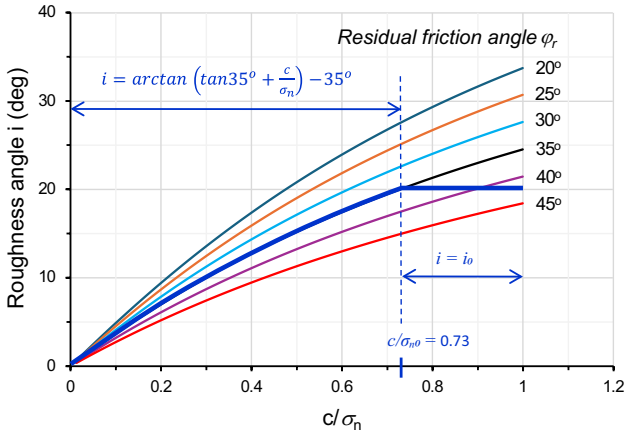

Fig. 17 Variation of roughness angle i versus cohesion–normal stress ratio for various residual friction angles. The lines and annotations highlighted in blue correspond to the example with $\varphi_r = 35°$ and $i_o = 20°$

should be noted that Barton (1976) proposed a shear strength criterion for rock joints that is similar to Eq. (10), although it employed the basic friction angle rather than the residual friction angle. In his subsequent studies, however, the basic friction angle was replaced by residual friction angle (Barton and Choubey 1977; Barton and Bandis, 1980). Within his criterion, Barton related the variable roughness angle, i, to the joint surface roughness (*JRC*), joint wall strength (*JCS*), and applied normal stress according to the following expression:

$$i = JRC \log 10\left(\frac{JCS}{\sigma_n}\right). \tag{16}$$

This expression describes the variation of the roughness angle over the range of $0 < \sigma_n \leq JCS$. When $\sigma_n = JCS$, the logarithmic term becomes zero, indicating that the joint asperities have been completely sheared off and no longer contribute to the shear resistance. A key advantage of the Barton criterion is that it relates the roughness angle to two joint surface parameters, both of which can be measured in engineering practice. Consequently, the criterion enables the shear strength of rock joints to be estimated directly from measured joint properties. Although the Barton criterion has been widely adopted since its introduction, the determination of parameters *JRC* and *JCS* remains a practical challenge. For example, Grasselli and Egger (2003) analyzed three randomly selected profiles from different rock samples of the same type of rock and estimated their *JRC* values through both visual comparison and back analysis. The considerable variability in the estimated values demonstrated that the currently available methods do not yield a unique or objective determination of *JRC*.

It must be noted that Eq. (15) derived in this study should not be interpreted as an alternative to, or direct replacement for, Barton's expression. Rather, it was developed solely to back-calculate the current roughness angle, i, in Eq. (10) from the regression line fitted to the experimental data. Therefore, a direct comparison between Eq. (15) and Barton's expression is not appropriate.

It is also noted that Ladanyi and Archambault (1969) attempted to develop a general failure model applicable to the full range of normal stresses for both irregular and regular joints. Their approach involves decomposing the shear force prior to asperity damage into three components, S_1, S_2, and S_3, and introducing an additional component, S_4, when asperity damage occurs. Two different friction angles are employed in the formulation of the first three components. However, the derivation procedure is open to question. In particular, the definition of the component S_2 in their derivation is not sufficiently clear and appears difficult to justify from a physical standpoint. Consequently, the physical interpretation underlying their proposed shear-resistance mechanism remains subject to debate.

5.4 Testing Facility

Triaxial testing of rock joints is easier to perform than direct shear testing. It can precisely measure normal and shear displacements of the joint in triaxial tests because the measurement LVDTs can be mounted directly on the rock specimen. On the contrary, normal and shear displacements are often measured on shear boxes in direct shear tests, which introduces erroneous displacements from the testing machine to the measurement (Larsson 2025). It is practically impossible to remove the erroneous displacements in the post-processing because they are often neither linearly related to the applied load nor to the displacement of the rock joint.

For rock joint tests, the triaxial chamber must be large enough to mount measurement LVDTs on the specimen. A Hoek cell can be used to test the shear strength of rock joints, but it cannot be used to determine normal and shear stiffness because the specimen cannot be subjected to hydrostatic pressure within the cell, and neither normal nor shear displacements of the joint can be measured directly on the specimen.

5.5 Applicability of the Triaxial Testing Method

The shear strength of rock joints, as well as their normal and shear stiffness, is known to be scale dependent, as demonstrated by Barton and Bandis (1980) and Grasselli and Egger (2003), among others. The investigation of scale effects is beyond the scope of the present study. Rather, the approach proposed in this paper provides a practical means of evaluating the mechanical properties of rock joints using available core specimens when rock joint samples cannot be obtained by other methods. Nevertheless, scale effects should be

carefully considered when test results derived from core specimens are applied to full-scale engineering projects.

In addition, the number of core specimens tested in this study is limited, and all specimens were obtained from two boreholes at a single site. It should be noted that rock joints with certain orientations may not be represented in core specimens if the boreholes are not appropriately oriented. In such cases, the test results may not adequately reflect the full range of mechanical properties of the rock joints present within the study area. Furthermore, the limitations associated with the use of core specimens should be carefully recognized when interpreting the results. Given the limited number of specimens and the restricted sampling coverage, the findings of this study should be further validated through additional testing on specimens collected from a broader range of geological settings and locations.

To date, this triaxial testing method has only been applied to hard rock core specimens. There is no reason to expect that the method would be invalid for weak rock joint specimens; however, its applicability to weak rock joints should be verified through future experimental studies.

6 Conclusions

The shear strength, shear stiffness, and normal stiffness of natural rock joints in diorite cores were successfully measured using triaxial testing. The shear strength is linearly related to the normal stress acting on the joint surface over a wide range of normal stresses (3–45 MPa). The residual friction angle of the rock joint surfaces ranges from 30.2° to 35° in most of the tested specimens, but reaches 36.7° and 37.7° in two specimens (B1 and C3) with relatively rough joint surfaces.

The friction failure criterion and Patton's bilinear failure criterion are linked in this study by establishing a relationship between the roughness angle in the friction failure criterion and the cohesion and residual friction angle in Patton's bilinear criterion.

The shear stiffness of the rock joints determined from the triaxial tests represents the average stiffness over a small range of normal stresses. The shear stiffness of the tested joints increased with increasing normal stress acting on the joint surface up to 15 MPa. Above 15 MPa, the shear stiffness remained constant.

The normal stiffness of rock joints can be readily determined from hydrostatic triaxial tests. The normal stiffness increases with increasing normal stress acting on the joint surface. The nonlinear relationship between them is well described by Goodman's hyperbolic expression.

The normal stiffness of rock joints can also be estimated from differential triaxial tests. However, caution is required when applying this approach, as the available portion of the normal stress–normal displacement curve for determination of normal stiffness is often short. Consequently, the determination may be subject to considerable uncertainty, making it difficult to obtain reliable estimates.

Appendix A. Images of Rock Joint Specimens

(see Figs. 18, 19, 20, 21, 22, 23, 24, 25).

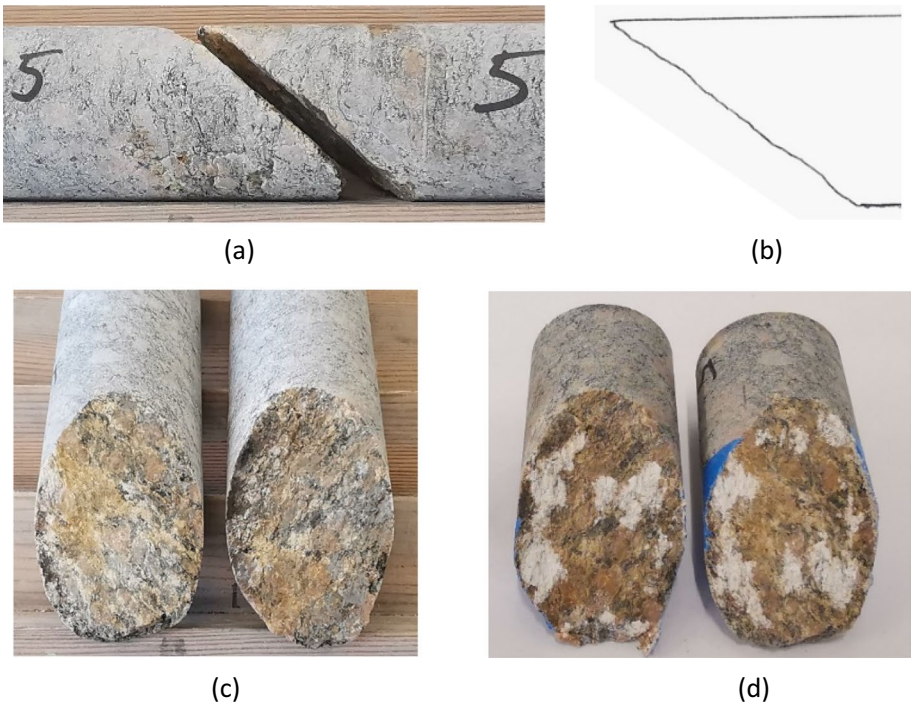

Fig. 18 Specimen A2 (joint angle $\alpha = 48.6°$): **a** the rock joint specimen, **b** JRC of the joint profile, **c** the joint surface before test, and **d** the joint surface after test

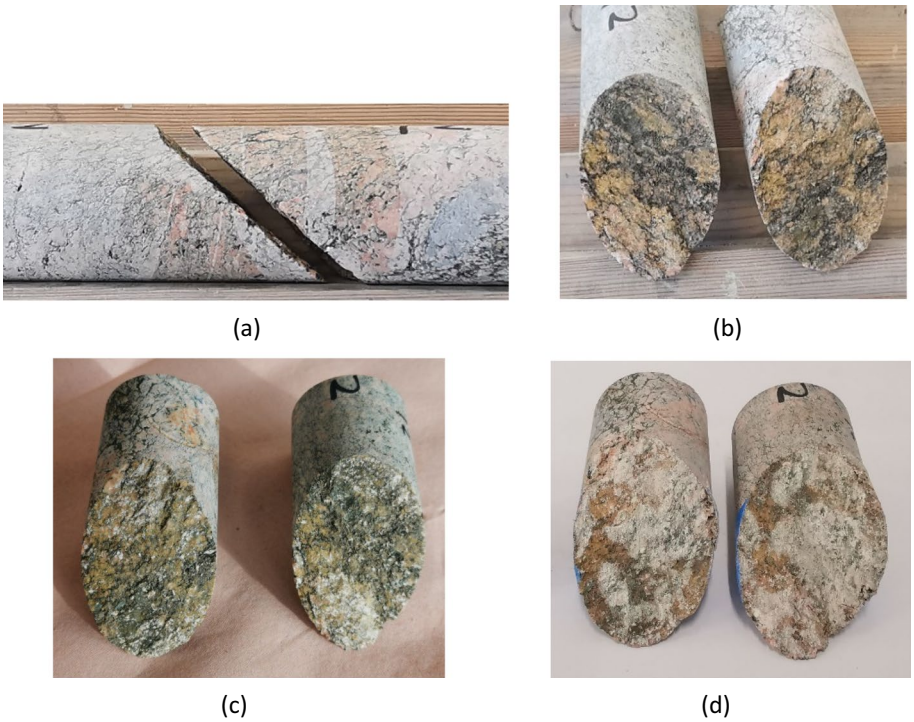

Fig. 19 Specimen A3 (joint angle $\alpha = 46.9°$): **a** the rock joint specimen, **b** the joint surface before test, **c** the joint surface after the first test, and **d** the joint surface after the second test

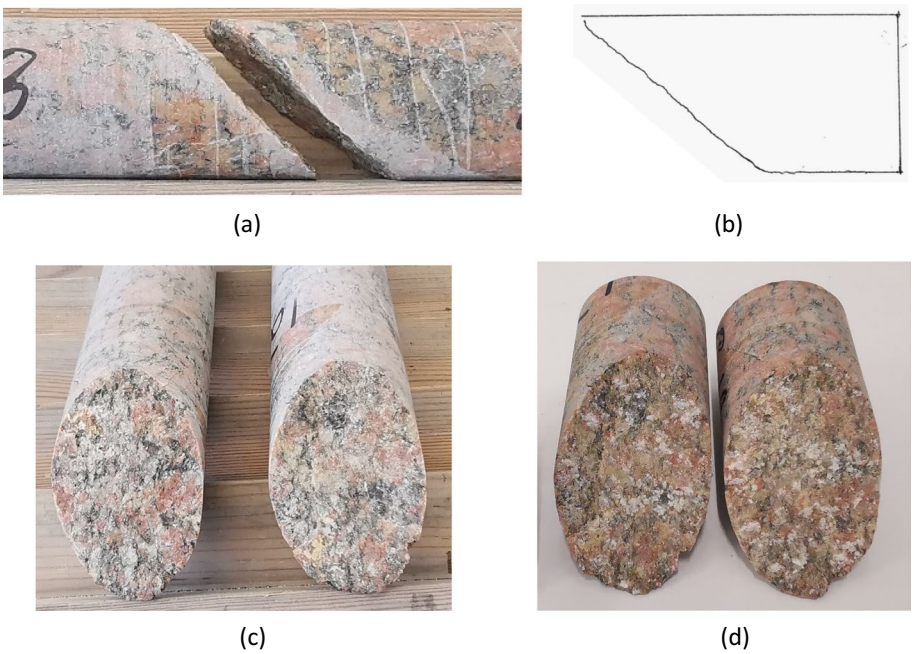

Fig. 20 Specimen B1 (joint angle $\alpha = 50.2°$): **a** the rock joint specimen, **b** JRC of the joint profile, **c** the joint surface before test, and **d** the joint surface after test

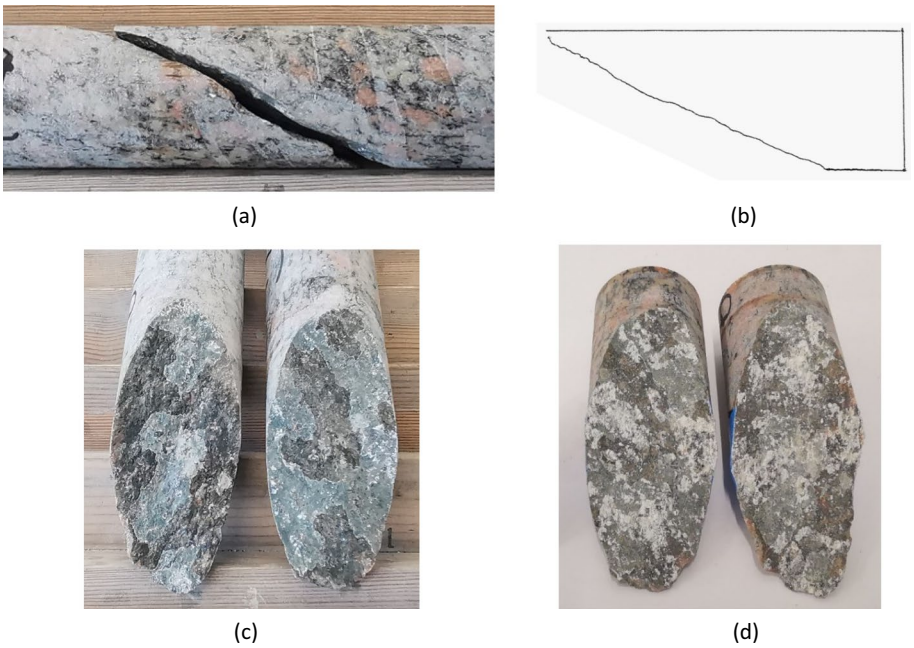

Fig. 21 Specimen B2 (joint angle $\alpha = 62.7°$): **a** the rock joint specimen, **b** JRC of the joint profile, **c** the joint surface before test, and **d** the joint surface after test

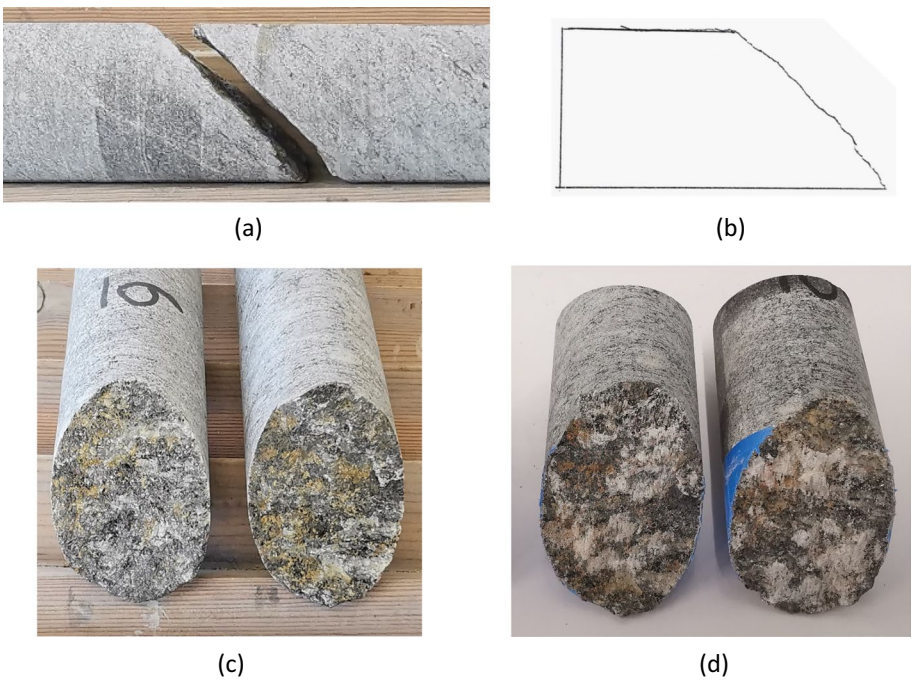

Fig. 22 Specimen C1 (joint angle $\alpha = 45.2°$): **a** the rock joint specimen, **b** JRC of the joint profile, **c** the joint surface before test, and **d** the joint surface after test

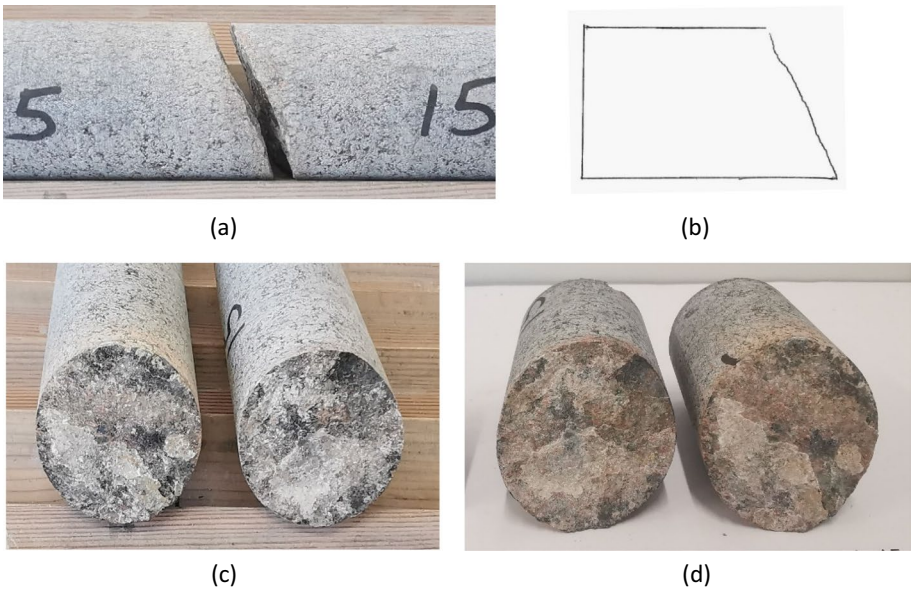

Fig. 23 Specimen C2 (joint angle $\alpha = 20.7°$): **a** the rock joint specimen, **b** JRC of the joint profile, **c** the joint surface before test, and **d** the joint surface after test

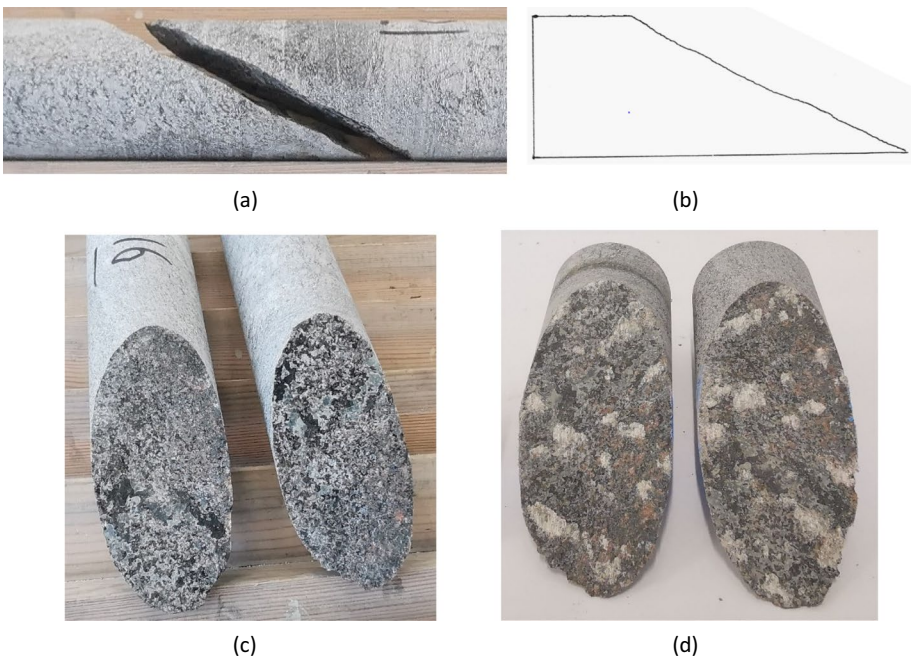

Fig. 24 Specimen C3 (joint angle $\alpha = 60.9°$): **a** the rock joint specimen, **b** JRC of the joint profile, **c** the joint surface before test, and **d** the joint surface after test

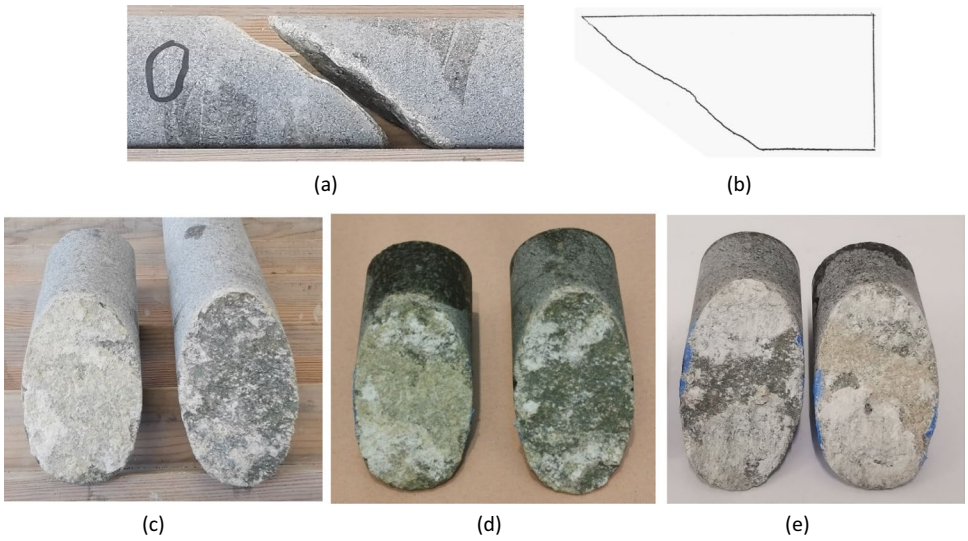

Fig. 25 Specimen C4 (joint angle $\alpha = 49.7°$): **a** the rock joint specimen, **b** JRC of the joint profile, **c** the joint surface before test, **d** the joint surface after the first test, and **e** the joint surface after the second test

Appendix B. Curves of Normal Stress vs. Normal Displacement And Normal Stiffness vs. Normal Stress in the Hydrostatic Triaxial Tests

(see Figs. 26, 27, 28, 29, 30, 31, 32).

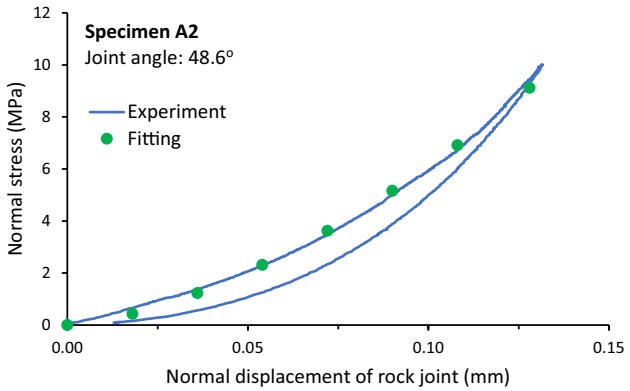

Fig. 26 Specimen A2: normal stress versus normal displacement and fitting by Eq. (12)

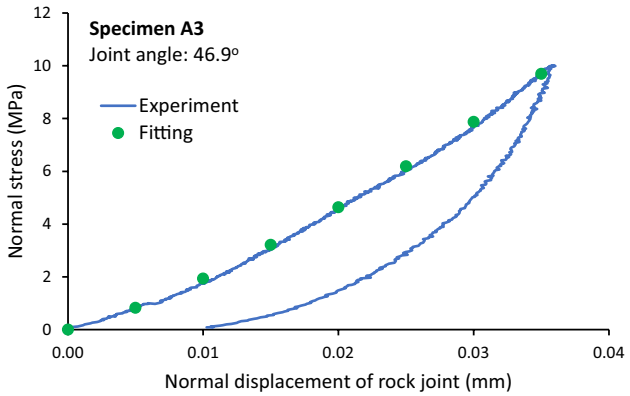

Fig. 27 Specimen A3: normal stress versus normal displacement and fitting by Eq. (12)

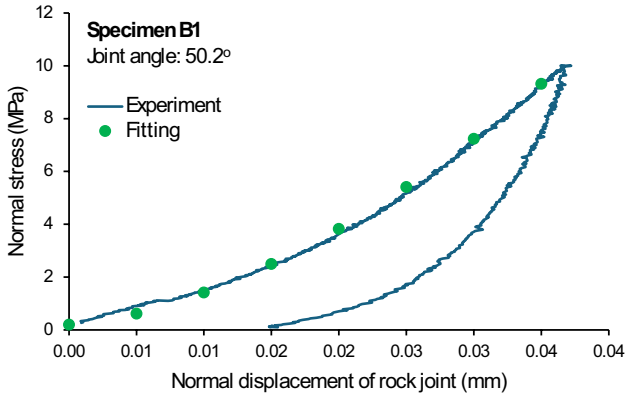

Fig. 28 Specimen B1: normal stress versus normal displacement and fitting b Eq. (12)

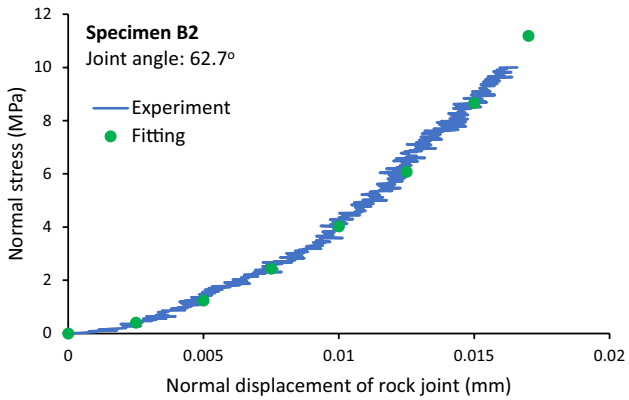

Fig. 29 Specimen B2: normal stress versus normal displacement and fitting by Eq. (12)

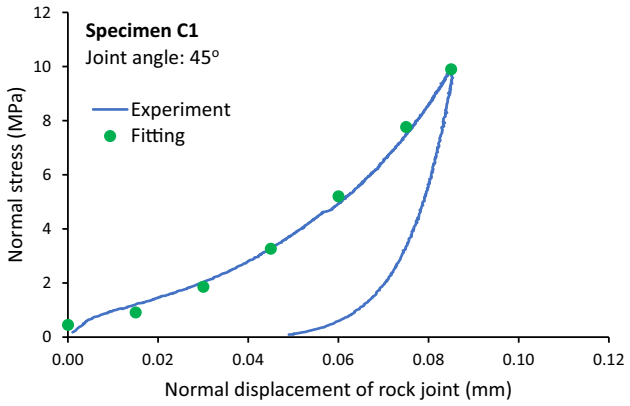

Fig. 30 Specimen C1: normal stress versus normal displacement and fitting by Eq. (12)

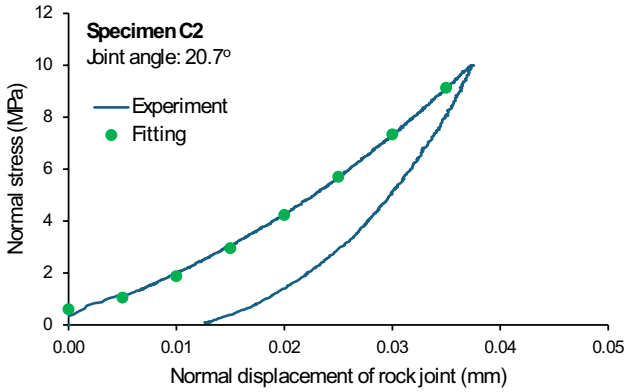

Fig. 31 Specimen C2: normal stress versus normal displacement and fitting by Eq. (12)

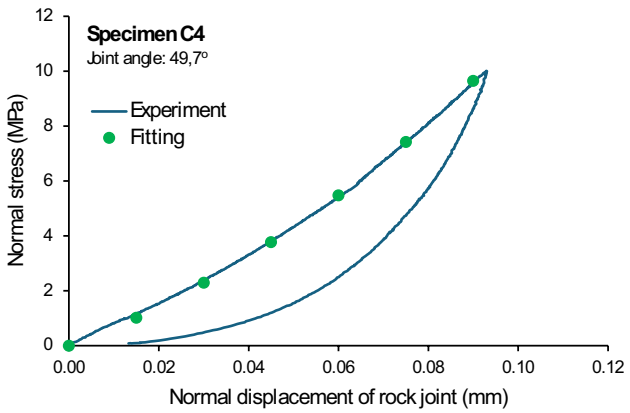

Fig. 32 Specimen C4: normal stress versus normal displacement and fitting by Eq. (12)

Appendix C. Curves of Shear Stress vs. Shear Displacement of the Tested Specimens in the Differential Triaxial Tests

(see Figs. 33, 34, 35, 36, 37, 38, 39, 40).

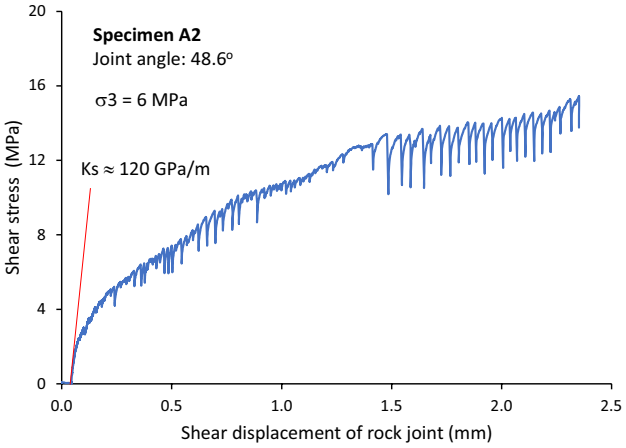

Fig. 33 Specimen A2: shear stress–displacement curves under confining stress of 6 MPa

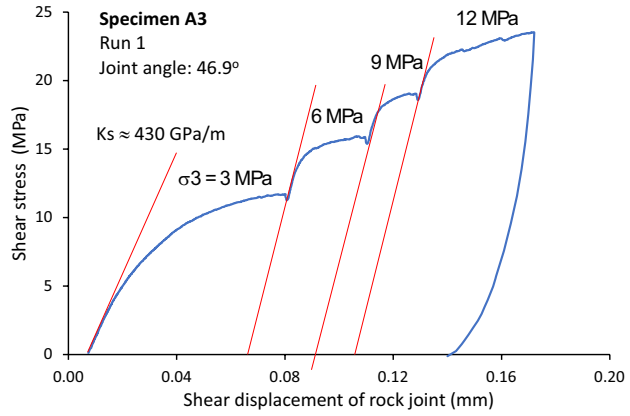

(a)

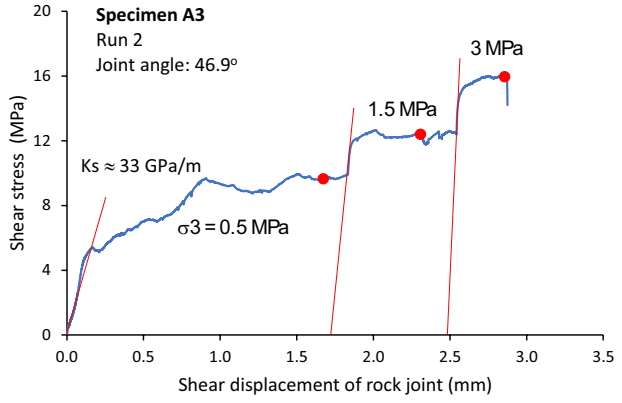

(b)

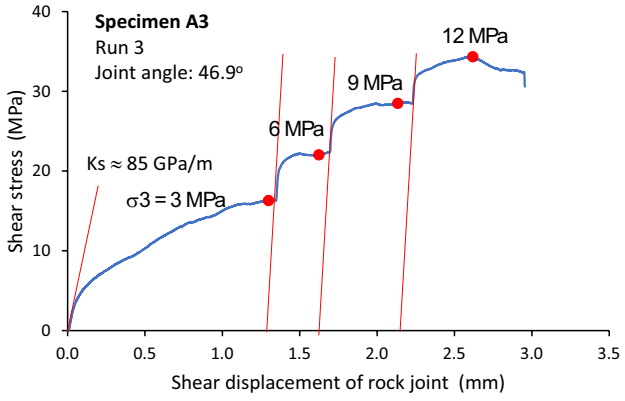

(c)

Fig. 34 Specimen A3: shear stress–displacement curves under various confining stresses from three test runs: **a** the first run, **b** the second run, and **c** the third run

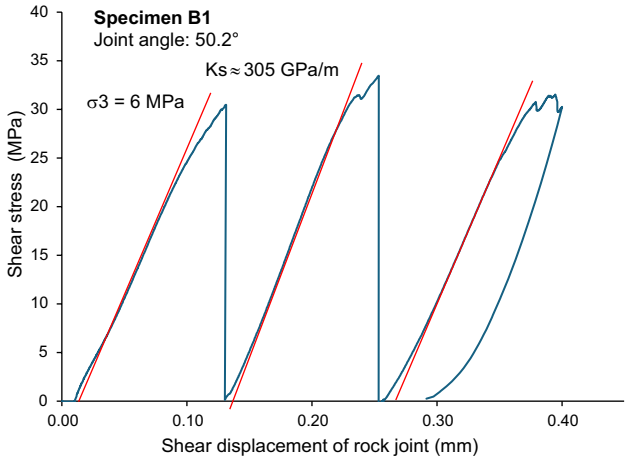

Fig. 35 Specimen B1: shear stress–displacement curves under confining stress of 6 MPa

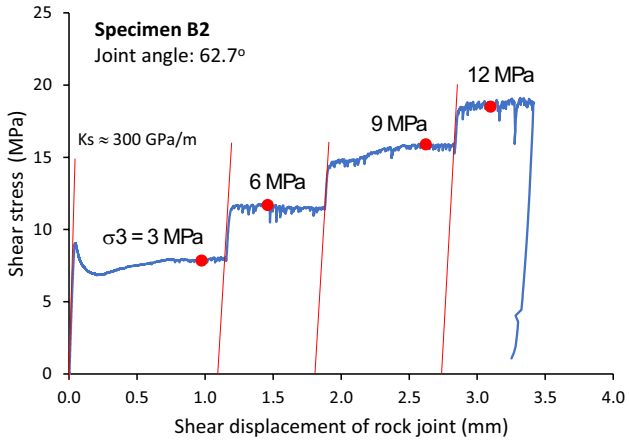

Fig. 36 Specimen B2: shear stress–displacement curves under four confining stresses

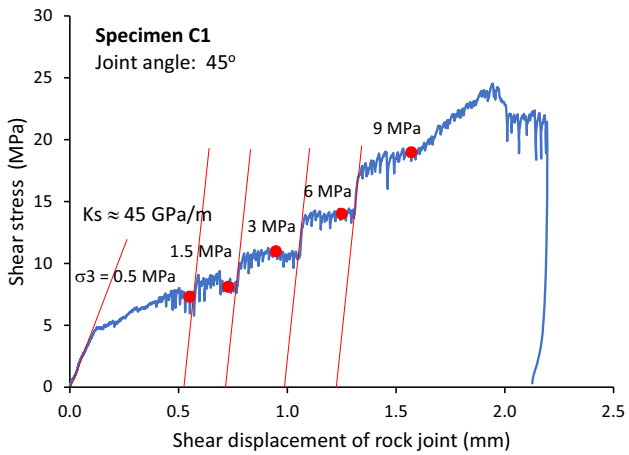

Fig. 37 Specimen C1: shear stress–displacement curves under five confining stresses

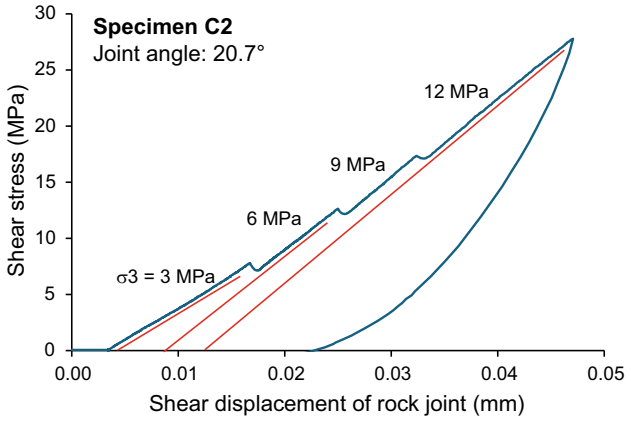

Fig. 38 Specimen C2: shear stress–displacement curves under four confining stresses

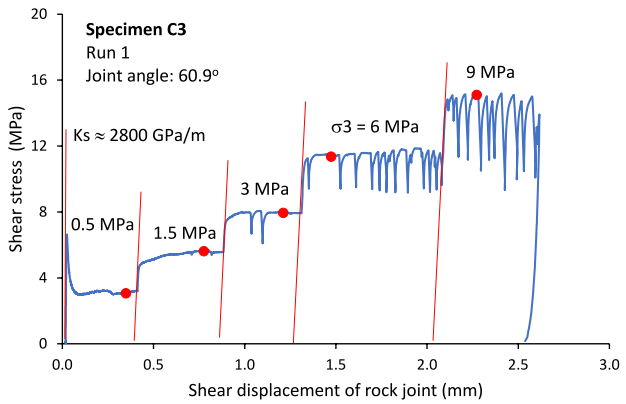

(a)

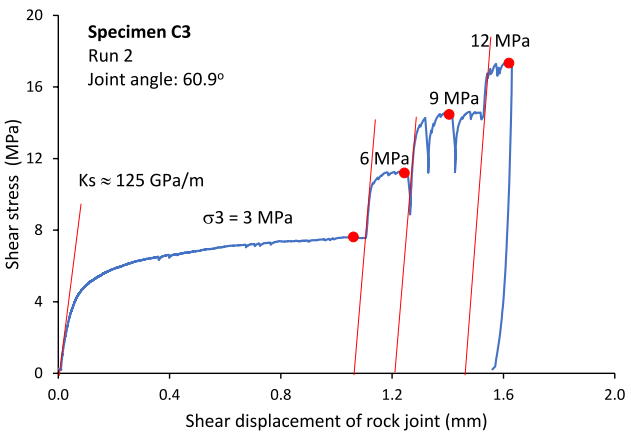

(b)

Fig. 39 Specimen C3: shear stress–displacement curves under various confining stresses from two test runs: **a** the first run and **b** the second run

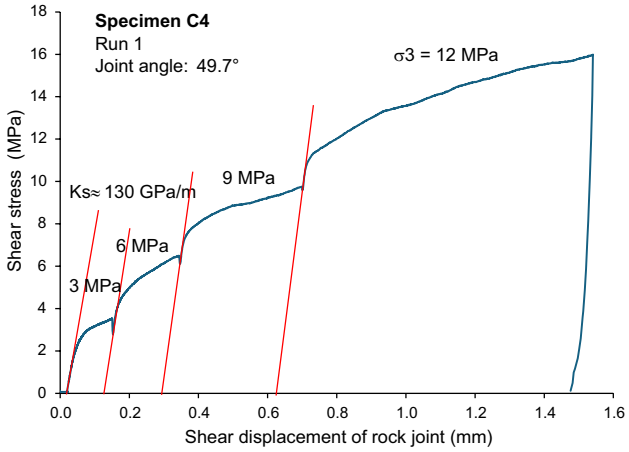

(a)

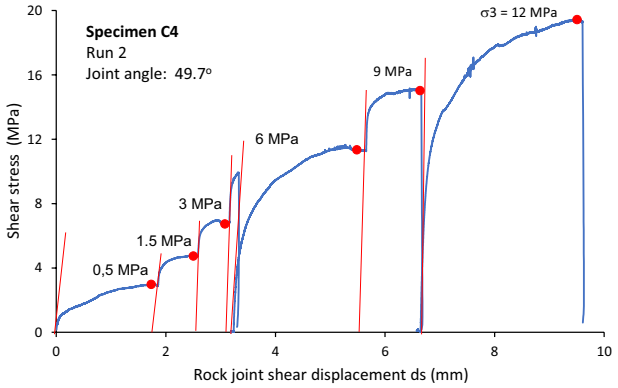

(b)

Fig. 40 Specimen C4: shear stress–displacement curves under various confining stresses from two test runs **a** the first run and **b** the second run

Appendix D. Curves of Shear Stress Versus Normal Stress on the Joint Plane

(see Figs. 41, 42, 43, 44, 45).

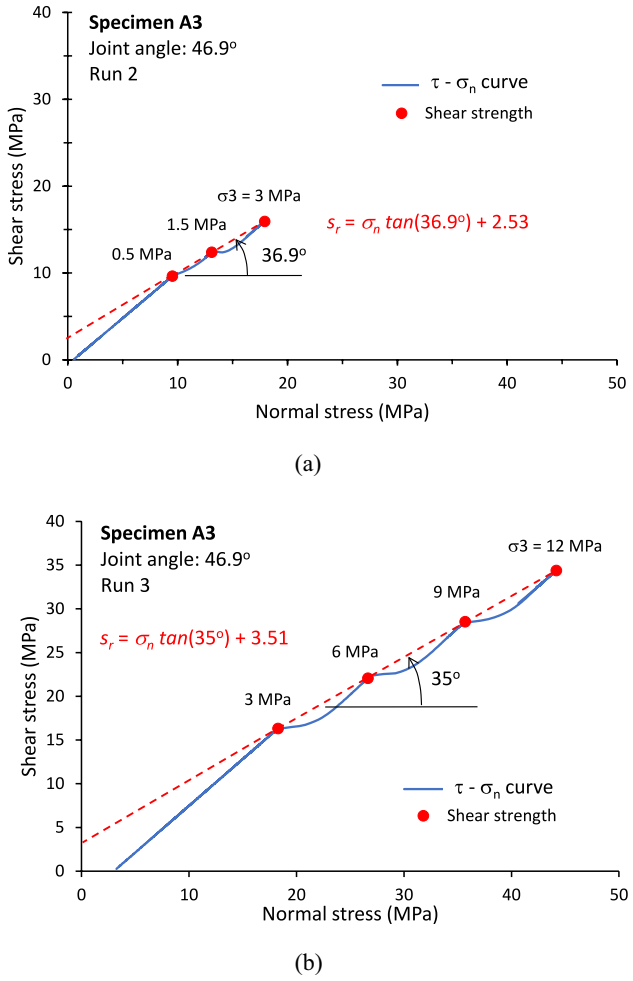

Fig. 41 Specimen A3: the shear stress versus the normal stress on the joint plane in **a** the second test and **b** the third test

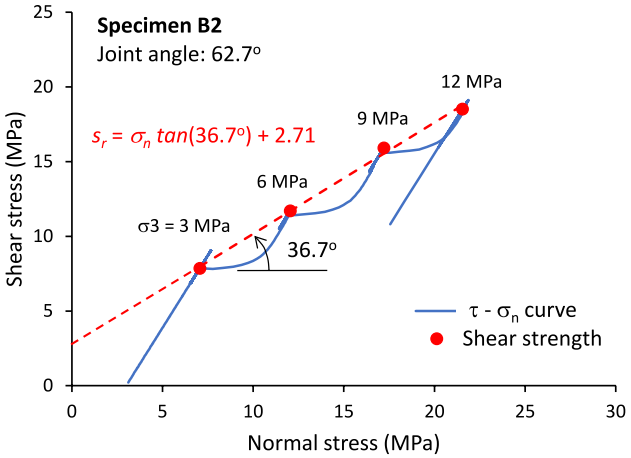

Fig. 42 Specimen B2: the shear stress versus the normal stress on the joint plane

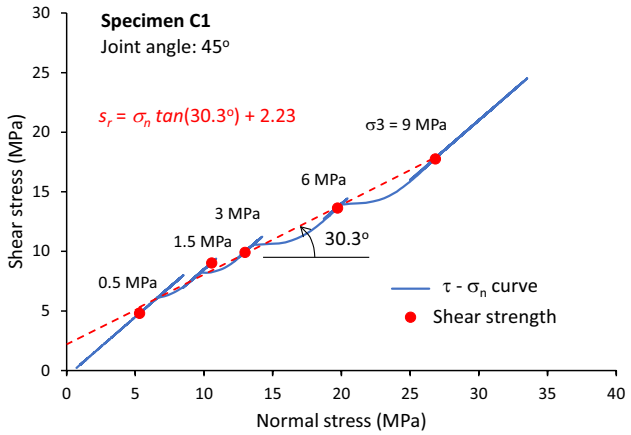

Fig. 43 Specimen C1: the shear stress versus the normal stress on the joint plane

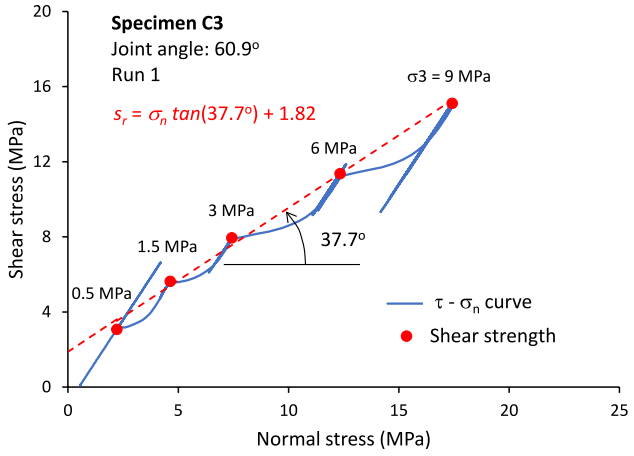

(a)

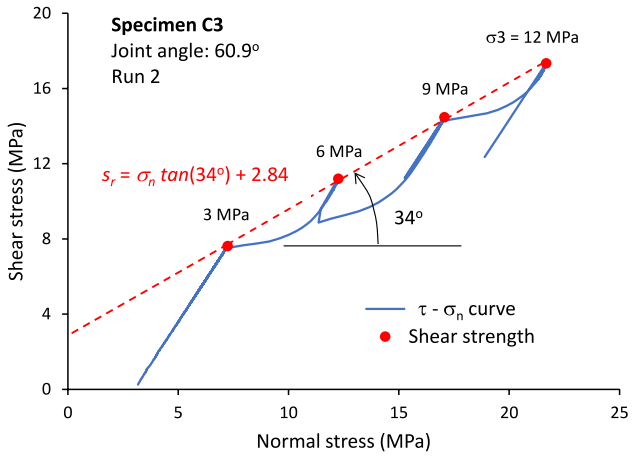

(b)

Fig. 44 Specimen C3: the shear stress versus the normal stress on the joint plane in **a** the first test and **b** the second test

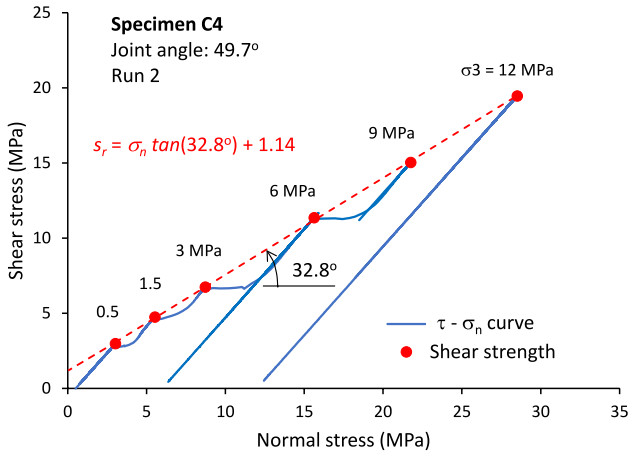

Fig. 45 Specimen C4: the shear stress versus the normal stress on the joint plane in the second test

Acknowledgements The authors gratefully acknowledge the funding from the project "Hydrogen, ammonia, and methanol in hydrogen hubs in the Nordic region (H2AMN)" funded by the Nordic Council of Ministers, through Nordic Energy Research (NER) (Project No. 2315912-0611), and a project of rock joint testing funded by the Norwegian Public Roads Administration (NPRA). The laboratory tests were carried out with the assistance of Mr. Jon Runar Drotninghaug. Mr. Brage Straume also contributed to the laboratory work.

Author Contributions Charlie C. Li: conceptualization, methodology, data curation, formal analysis, visualization, validation, investigation, funding acquisition, resources, writing—original draft. Ping Zhang: data curation, formal analysis, investigation, project administration, writing—review and editing. Are Håvard Høien: curation, formal analysis, investigation, funding acquisition, writing—review and editing.

Funding Open access funding provided by NTNU Norwegian University of Science and Technology (incl St. Olavs Hospital - Trondheim University Hospital). Nordic Energy Research, 2315912-0611.

Data Availability Additional data readers are interested in are available by contacting the corresponding author.

Conflict of interest The authors have no conflict of interest.

Open Access This article is licensed under a Creative Commons Attribution-NonCommercial-NoDerivatives 4.0 International License, which permits any non-commercial use, sharing, distribution and reproduction in any medium or format, as long as you give appropriate credit to the original author(s) and the source, provide a link to the Creative Commons licence, and indicate if you modified the licensed material. You do not have permission under this licence to share adapted material derived from this article or parts of it. The images or other third party material in this article are included in the article's Creative Commons licence, unless indicated otherwise in a credit line to the material. If material is not included in the article's Creative Commons licence and your intended use is not permitted by statutory regulation or exceeds the permitted use, you will need to obtain permission directly from the copyright holder. To view a copy of this licence, visit http://creativecommons.org/licenses/by-nc-nd/4.0/.

References

Arzúaa J, Alejano LR, Walton G (2014) Strength and dilation of jointed granite specimens in servo-controlled triaxial tests. Int J Rock Mech Min Sci 69:93–104

Bandis SC, Lumsden AC, Barton NR (1981) Experimental studies of scale effects on the shear behaviours of rock joints. Int J Rock Mech Min Sci Geomech Abstr 18:1–21

Bandis SC, Lumsden AC, Barton NR (1983) Fundamentals of rock joint deformation. Int J Rock Mech Min Sci Geomech Abstr 20(6):249–268

Barton N (1976) The shear strength of rock and rock joints. Int J Rock Mech Min Sci Geomech Abstr 13:255–279

Barton N, Bandis S (1980) Some effects of scale on the shear strength of joints. Int J Rock Mech Min Sci & Geomech Abstr 17:69–73

Barton N, Bandis S (1990) Review of predictive capabilities of JRC-JCS model in engineering practice. Rock joints. Balkema, Rotterdam, pp 603–610

Barton N, Choubey V (1977) The shear strength of rock joints in theory and practice. Rock Mech 10(1):1–54

Bieniawski ZT, Bernede MJ (1979) Suggested methods for determining the uniaxial compressive strength and deformability

of rock materials. Int J Rock Mech Min Sci Geomech Abstr 16(2):137–140

Bjurstrom S (1974) Shear strength of hard rock joints reinforced by grouted untensioned bolts. In: Proc. 3rd ISRM Congress

Cano M, Pastor JL, Cabrera H, Buzon L, Miranda T (2024) Assessing of influence of heterogeneity on the shear strength oj joints: an experimental study using artificial stone materials. In: Proc. EUROCK 2024 – New Challenges in Rock Mechanics and Rock Engineering. 645–650

Gonzalez-Fernandez MA, Alejano LR, West IG, Walton G (2024) Strain analysis and joint stiffness estimation based on jointed granite specimens submitted to triaxial tests. In: Proc. EUROCK 2024 – New Challenges in Rock Mechanics and Rock Engineering. 696–702

Goodman RE (1976) Methods in geological engineering in discontinuous rocks. West, St Paul (**ISBN 0-8299-0066-7**)

Goodman RE (1980) Introduction to rock mechanics, 1st edition. Wiley, New York

Goodman RE, Ohnishi Y (1973) Undrained shear testing of jointed rock. Rock Mech 5:129–149

Grasselli G, Egger P (2003) Constitutive law for the shear strength of rock joints based on three-dimensional surface parameters. Int J Rock Mech Min Sci 40:25–40

Ladanyi B, Archambault G (1969) Simulation of shear behaviour of a jointed rock mass. *ARMA US Rock Mechanics/Geomechanics Symposium*, Chapter 7. pp 109–125

Lane KS, Heck WJ (1964) Triaxial testing for strength of rock joints. In: The 6th U.S Symposium on Rock Mechanics (USRMS*)*, Rolla, Missouri, October 1964. Paper Number: ARMA-64–098.

Larsson J (2021) Experimental investigation of the system normal stiffness of a 5 MN direct shear test setup and the compensation of it in CNS direct shear tests. IOP Conf. Ser.: Earth Environ. Sci. 833–012011

Larsson J (2025) Approaches for increased accuracy in laboratory direct shear testing. *Doctoral Thesis TRITA-ABE-DLT-251*, Royal Institute of Technology, Sweden. ISBN 978–91–8106–205–2.

Larsson J, Flansbjer M (2020) An approach to compensate for the influence of the system normal stiffness in CNS direct shear tests. Rock Mech Rock Eng 53:2185–2199

Leichnitz W (1985) Mechanical properties of rock joints. Int J Rock Mech Min Sci Geomech Abstr 22(5):313–321

Muralha J, Grasselli G, Tatone B, Blume M, Chryssanthakis P, Yujing J (2014) ISRM suggested method for laboratory determination of the shear strength of rock joints: revised version. Rock Mech Rock Eng 47:291–302

Patton FD (1966) Multiple modes of shear failure in rock, Kin: Proc. Ist ISRM Congress, Lisbon. Vol. 1, 509–513

Reik G, Zacas M (1978) Strength and deformation characteristics of jointed media in true triaxial compression. Int J Rock Mech Min Sci Geomech Abstr 15:295–303

Rios-Bayona F, Johansson F, Mas-Ivars D (2021) Prediction of peak shear strength of natural, unfilled rock joints accounting for matedness based on measured aperture. Rock Mech Rock Eng 54(3):1533–1550

Shan R, Liu N, Sun P, Zhao Z, Dong R, Dou H (2025) Experimental and numerical simulation study of rough jointed rock samples under triaxial compression conditions. Eng Fract Mech 314:110707

Sun Z, Gerrard C, Stephansson O (1985) Rock joint compliance tests for compression and shear loads. Int J Rock Mech Min Sci Geomech Abstr 22(4):197–213

Wang Z-Y, Duan P-J (2011) A new method for determining mechanical parameters of joints based on triaxial compressive test for rock mass. Rock Soil Mech 32(11):3219–3224 ((**in Chinese**))

Wang SC, Yang XX, Li WT, Qiao WG (2023) Influence of a rock bridge on the shearing behavior of nonpersistent rough joints: an experimental study. Rock Mech Rock Eng 56:2573–2588

West IG, Walton G, Gonzalez-Fernandez MA, Alejano LR (2023) Strain localization in jointed rockmass analog laboratory specimens under compression. ARMA 23–0073:10p

Zhang X, Jiang Q, Chen N, Wie W, Feng X (2016) Laboratory investigation on shear behavior of rock joints and a new peak shear strength criterion. Rock Mech Rock Eng 49:3495–3512

Zhao J (1997) Joint surface matching and shear strength part A: joint matching coefficient (JMC). Int J Rock Mech Min Sci 34(2):173–178

Publisher's Note Springer Nature remains neutral with regard to jurisdictional claims in published maps and institutional affiliations.